scientific reports

Check for updates

OPEN

Microbial communities and biomineralization potential within mountain permafrost of the Devaux ice cave in the Central Pyrenees

Víctor Muñoz-Hisado[1,2], Miguel Bartolomé[3], M. Cinta Osácar[4], Reyes Giménez[5], Gerard Cazenave[6], Eva Garcia-Lopez[1], Ana Moreno[5] & Cristina Cid[1]✉

Ice caves constitute one of the last cryospheric environments studied in the meridional regions. They are undergoing a pronounced ice reduction, and are an important example of ecosystems that have not yet been thoroughly explored from a microbiological point of view. The Devaux cave, in the Central Pyrenees, still hosts perennial ice. To test whether this ice contained microbial communities, prokaryotic and eukaryotic microorganisms were searched by sequencing their 16S and 18S rRNA genes. From the taxonomic information, the potential functional pathways of these communities were predicted using bioinformatic techniques. In addition, the genome of the microorganisms housed in the perennial ice samples was investigated, and through metagenomic studies their metabolic capacity was elucidated. The cryogenic mineralization of the Devaux cave leads to the production of various Ca and Mg carbonates: calcite, aragonite, vaterite, Mg-rich calcite, and nesquehonite, whose formation may have been favored by the microorganisms in the cave. Among the genes encoding enzymes that enable reactions involved in biomineralization, those belonging to the nitrate and sulfate reduction dissimilatory pathways as well as ureases, ammonia lyases, and carbonic anhydrases were identified. This research takes a further step in the investigation of biomineralization, using the Devaux cave as a model.

Keywords Ice cave, Permafrost, Biomineralization, Microbial communities, Cryogenic cave carbonates, Metataxonomy, Metagenomics, Biogeochemistry

Abbreviations

ASVs	Amplicon sequence variants
BIMP	Bacteria-induced mineral precipitation
CCA	Canonical correspondence analysis
CCC	Cryogenic cave carbonates
EDS	Energy dispersive X-ray spectrometry
EPS	Extracellular polymeric substance
KEGG	Kyoto encyclopedia of genes and genomes
KO	KEGG orthology
FE-SEM	Field emission scanning electron microscopy
MAGs	Metagenome-assembled genomes

[1]Centro de Astrobiología (CAB), CSIC-INTA, Carretera de Ajalvir km4, Torrejón de Ardoz, 28850 Madrid, Spain. [2]2Escuela de Doctorado de la Universidad Autónoma de Madrid, Centro de Estudios de Posgrado, Ciudad Universitaria de Cantoblanco, 28049 Madrid, Spain. [3]Departamento de Geología, Museo Nacional de Ciencias Naturales (CSIC), C. de José Gutiérrez Abascal 2, 28006 Madrid, Spain. [4]Departamento de Ciencias de la Tierra, Instituto Universitario de Ciencias Ambientales y Grupo GeoTransfer, Universidad de Zaragoza, C. de Pedro Cerbuna 12, 50009 Zaragoza, Spain. [5]Departamento de Procesos Geoambientales y Cambio Global, Instituto Pirenaico de Ecología - CSIC, 50059 Zaragoza, Spain. [6]Société de Spéléologie et de Préhistoire des Pyrénées Occidentales (SSPPO), 5 Allée du Grand Tour, 64000 Pau, France. ✉email: cidsc@cab.inta-csic.es

PCoA	Principal coordinate analysis
XRD	X-ray diffraction

The cryosphere in the meridional regions is undergoing a pronounced ice reduction. In the case of the Pyrenees, glaciers will disappear in the coming decades according to temperature increase projections[1]. Glaciers are not the only components of the cryosphere threatened by global warming; permafrost and ice caves are also at risk[2]. Ice caves, in particular, remain poorly characterized environments. These environments are defined as rock caves that host perennial ice resulting from the diagenesis of snow and/or the freezing of infiltrating water reaching the cave[3]. Ice caves serve as reservoirs capable of preserving ice for millennia[4,5]. Thus, these environments have attracted great interest as unique archives to study past climatic conditions[6–12], as well as paleoecological[13,14] and microbiological studies[15].

Ice caves represent a largely unexplored ecosystem from a microbiological point of view, as they contain vast "microbial dark matter," i.e., unknown microbial diversity[16]. Although recent studies[17] have begun to address these environments, limited accessibility and protected area status often restrict research. This isolation, however, can preserve these habitats from human impact, making them valuable reservoirs of unique genetic resources[18,19]. Ice cave research is increasingly relevant to understanding ecological processes, discovering bioactive compounds of industrial interest[20], and developing sampling and analytical methods applicable to space exploration[21]. Studies indicate that cave ice deposits harbor microorganisms that remain viable at sub-zero temperatures, being the only inhabitants that maintain active biogeochemical cycles[15,22]. Ice caves provide unique microclimatic conditions that favor the development of secondary minerals. These environments, characterized by low temperatures, high humidity, and limited nutrient availability, create ecological niches such as ice-rock interface films, cryogenic brines, cryogenic cave carbonates, and mineral surfaces (calcite, gypsum) that support psychrophilic, oligotrophic microbial communities[22–24]. Recent studies have shown that many secondary minerals, previously considered purely inorganic, may result from microbial mediation. In particular, bacterial-induced mineral precipitation (BIMP) plays a significant role in the formation of calcic minerals such as calcite and aragonite, contributing to the genesis of speleothems within these cryogenic settings[17,25,26]. Biomineralization processes are due to several metabolic pathways that favor carbonate precipitation in the presence of divalent cations such as Mg^{2+} or Ca^{2+}[27]. Therefore, these processes can be defined as extracellular induced biomineralization, as they are not intracellular processes as for example the magnetite formation by magnetotactic bacteria[27]. In carbonate biomineralization, cell surface molecules and extracellular polymeric substance (EPS) play a key role because they act as nucleation site for the growing crystal[28]. Several metabolic pathways are known to be involved in carbonate precipitation, such as autotrophic photosynthesis, ammonification, ureolysis, dissimilatory reduction of nitrates and sulfates, as well as methane oxidation[29,30]. These biochemical routes are responsible for changes in the cell microenvironment that favor salt supersaturation and thus biomineralization[17]

Cryogenic cave carbonates (CCC) have emerged as sensitive indicators of permafrost thaw and/or cave-ice formation, because their grain sizes, textures, and stable-isotope signatures directly record freezing kinetics and the mass balance of subterranean ice bodies[23,31–35]. CCC form when seepage or ponded karst water freezes, a process that excludes solutes and promotes CO_2 degassing[23]; the resulting chemical evolution of the residual liquid drives supersaturation and carbonate precipitation (and at times sulfates) under cryogenic conditions[35–37].

The system dynamics govern which CCC type develops. In open systems with rapid freezing and continuous CO_2 exchange with the cave atmosphere, CCC_{fine} typically forms (fine, powdery aggregates that exhibit strong kinetic isotope effects). In semi-closed systems, slow freezing can seal the water surface with an ice lid, maintaining a liquid lens beneath; gradual degassing and progressive solute enrichment favor growth of CCC_{coarse}, characterized by larger crystals and near-equilibrium isotope signatures[23,38]. Recent observations from Austrian alpine ice caves also point to an intermediate category ($CCC_{intermediate}$), fine grain sizes (< 1 mm) but stable-isotope values overlapping CCC_{coarse}, consistent with freezing and degassing rates between the classical end members[38].

Although CCC formation has usually been treated as purely inorganic, cave geomicrobiology demonstrates that biofilms can nucleate and modulate carbonate precipitation on mineral surfaces, raising the hypothesis that microbial communities may influence CCC textures and morphologies in specific microhabitats[34,39]. In Hawaiian lava-tube ice caves, CCC-bearing deposits host diverse communities dominated by Actinobacteria and Proteobacteria, groups frequently implicated in biomineralization and carbonate nucleation[40]. Complementarily, a study in Winter Wonderland Cave (Utah, USA) that sampled ice, liquid water, and exposed CCC reported higher cell counts in liquid water than in ice, with the highest bacterial diversity in CCC; microscopy revealed coccoid/bacillus morphologies in water and calcite spherules or possible cells in CCC[24]. These findings support a model in which microbes concentrate in the liquid layer, settle, and co-precipitate with CCC, either supplying nutrients or reflecting direct biomineralization[24]. Taken together, these lines of evidence support a process-to-proxy framework: freezing kinetics (open vs. semi-closed) regulate CCC type, while microbial communities may modulate nucleation and growth at the ice-water interface, within cryogenic brines, and on mineral surfaces. This coupling strengthens the use of CCC as paleocryospheric indicators and underscores the need for targeted microbiological investigations to quantify the role of biomineralization in their genesis[23].

This study examines the cryogenic mineralogy and compares the microbial communities inhabiting Devaux Cave under three distinct hydrological conditions: perennial ice, seasonal ice, and liquid water (Figs. 1, 2). Additionally, it explores the metabolic potential of these microorganisms, focusing on pathways that may influence bacterial-induced mineral precipitation (BIMP). The ice deposits in Devaux Cave offer exceptional insights into the processes driving cryogenic mineral formation and provide a unique natural laboratory for investigating biomineralization within the mountain permafrost of the Pyrenees.

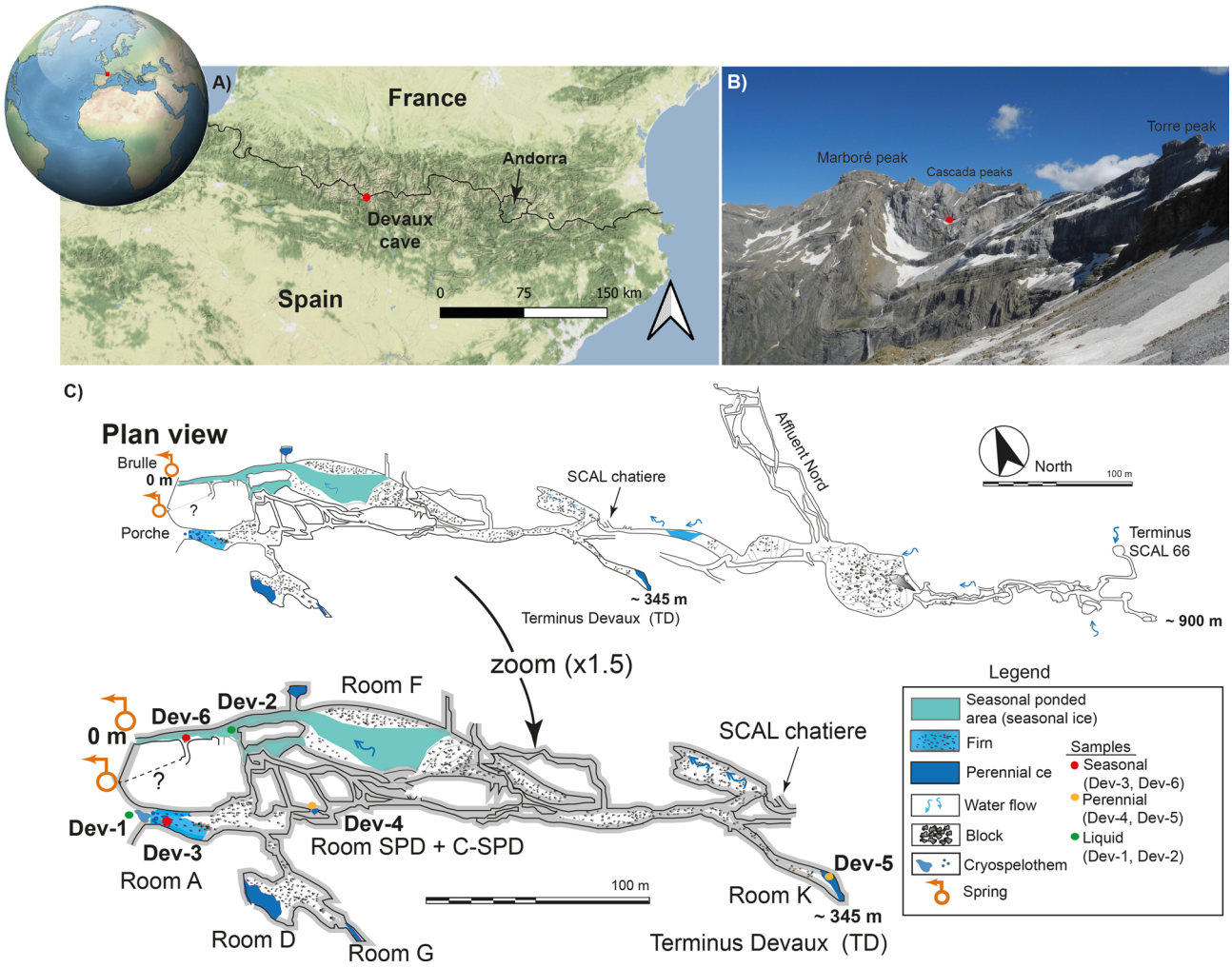

Fig. 1. (**A**) Location of Devaux cave in the Central Pyrenees (ASTER GDEM, NASA v3, 2019). Maps were created using Stamen Design basemap (http://maps.stamen.com), which uses OpenStreetMap data under the Open Database License (ODbL) in QGIS (https://qgis.org/). (**B**) Gavarnie cirque**.** Picture of the Gavarnie cirque (France) and main peaks closed to Devaux cave (red dot) (Photo taken by: Gerard Cazenave from Sarradets hut, France). (**C**) Plan view**.** Plan view of the Devaux cave, and the enlarged area corresponding to the first ~ 345 m showing the locations of samples (liquid, seasonal ice and perennial ice) and the main cave deposits. Figure was generated using Inkscape (https://inkscape.org/), an open-source vector graphics editor, based on topographical data from the cave survey. Original cave survey by Marc Galy, Groupe Spéléologique des Pyrénées (GSPY 86).

Results and discussion

Chemical properties of ice and water

The elemental and ionic composition of Devaux Cave samples was quantified (Table S1), and the following variables were explicitly compared: calcium (Ca), magnesium (Mg), bicarbonate alkalinity (HCO_3^-), sulfate (reported as S for SO_4^{2-}), and total carbon (together with any additional elements listed in Table S1). An ANOVA was applied and showed significant differences among all samples (*$p < 0.0001$; Fig. S1). Although Newman-Keuls multiple comparisons did not detect significant differences among replicate groups ($p > 0.05$), two clusters were apparent in Fig. S1: liquid river water (DEV-1, DEV-2) versus ice (DEV-3 to DEV-6). A Student's t-test confirmed significant differences between these two groups (##$p = 0.004$). Pairwise comparisons indicated that the river water samples (DEV-1, DEV-2) were highly similar, whereas the perennial ice samples (DEV-4, DEV-5) differed markedly. By contrast, DEV-5 and DEV-6 exhibited comparable chemical profiles, a result interpreted as likely related to their elevated carbon content. Taken together, phase (liquid vs. ice) was observed to act as the primary driver of chemical separation in Devaux Cave, with carbon and major-ion chemistry contributing to the differentiation (Table S1; Fig. S1).

In Pyrenean karst systems, water chemistry was reported to be dominated by Ca-Mg-HCO_3^-, with sulfate contributions arising from gypsum dissolution and oxidation processes[41]. For Devaux Cave, waters were described as Ca- and HCO_3^--rich, with relatively high Mg, and locally elevated sulfate, particularly in drip water compared with river water; $\delta^{34}S$ data were interpreted to implicate pyrite oxidation as a sulfate source[6,41]. The

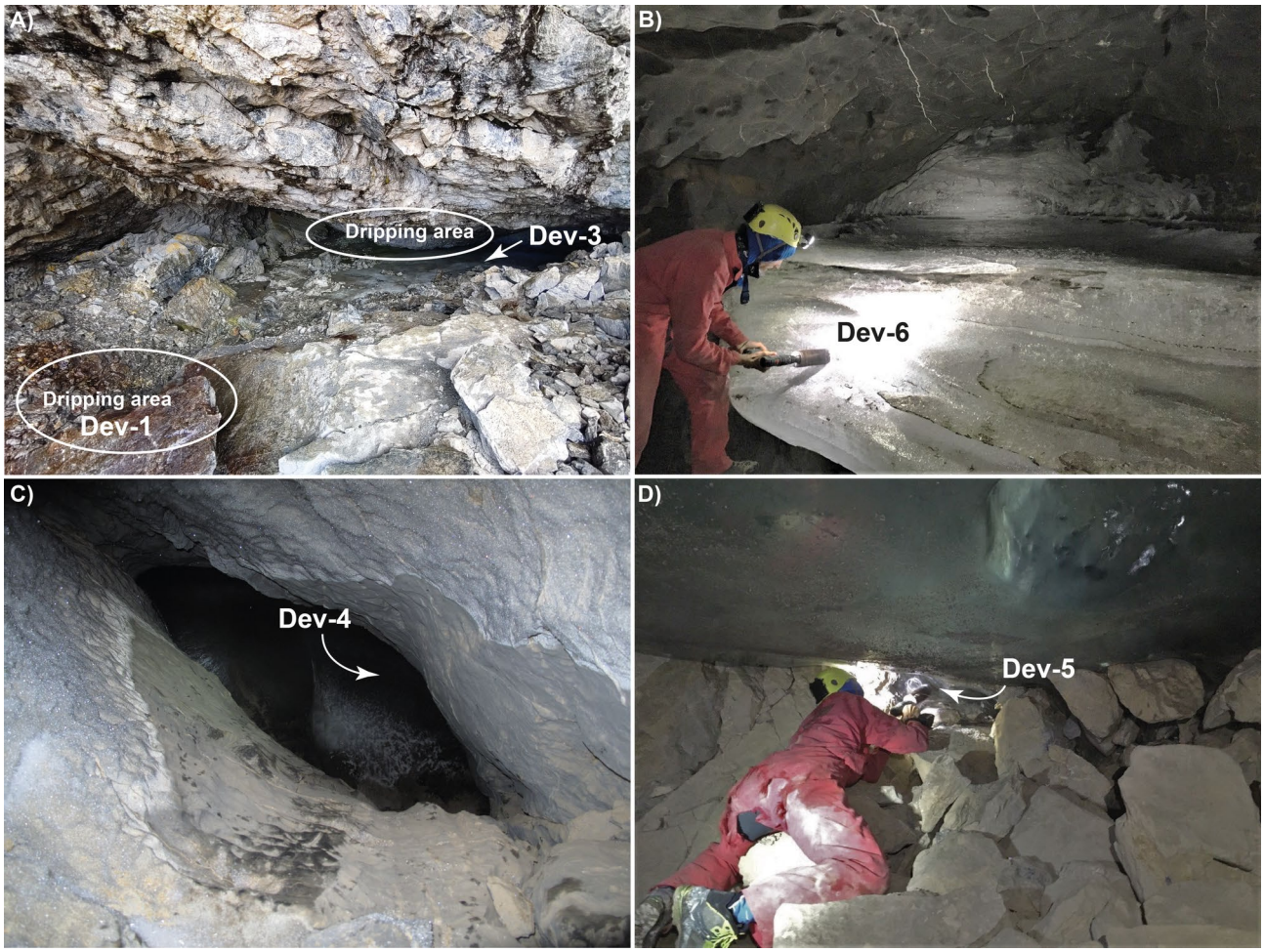

Fig. 2. (**A**) Porche entrance and the location of the sample DEV-3 taken from the firn, and dripping areas (white ellipsoids). (**B**) Sampling ice from seasonal ice formed during late winter/early spring 2022 in the gallery between room F and Brulle Spring. (**C**) Room SPD and location of the sample DEV-4 in the perennial ice. (**D**) Sampling (DEV-5) in the ice located in room K. Samples DEV-1 and DEV-2 correspond with drip water and river water respectively.

water–ice separation and the carbon-associated clustering observed here were consistent with those earlier observations[6], while the explicit comparison of Ca, Mg, HCO_3^-, SO_4^{2-} (as S), and total carbon clarified the variables underpinning the statistical differences reported for Devaux Cave (Table S1; Fig. 1).

Mineralogical and chemical composition and micromorphology of the CCC samples

X-ray diffraction in an aliquot of CCC collected in the room SPD and room C-SPD, showed the presence of diverse carbonates: the three polimorphs of $CaCO_3$ (calcite, aragonite and vaterite), Mg-rich calcite, and nesquehonite ($MgCO_3 \cdot 3H_2O$) (Fig. S2). Calcite and aragonite were the most abundant; vaterite, Mg-ric calcite and nesquehonite were occasional. Chemical analyses by EDS confirmed this composition and showed the absence of Fe in these carbonates, as it can be observed in the spectrum in Fig. S2C.

The Field Emission Scanning Electron Microscopy (FE-SEM images of CCC reveal structures that strongly suggest a biological influence on mineral formation (Fig. 3A–E). Similar features have been documented in other cave environments, where biomineralization processes driven by microbial activity play a key role in carbonate precipitation[27,28,42]. Microorganisms can induce mineralization through metabolic pathways that alter local geochemistry, such as increasing alkalinity or providing nucleation sites, resulting in distinctive morphologies[43]. In our samples, spheroidal and globular $CaCO_3$ morphologies (Fig. 3A–D) are particularly noteworthy, as these forms are commonly associated with microbial mediation[44,45]. Such structures often arise from extracellular polymeric substances (EPS) produced by microbes, which trap ions and facilitate crystal growth in a controlled microenvironment. This interpretation aligns with previous studies linking globular carbonate aggregates to biofilm activity in karst systems[28]. Needle-like fibrous crystals were also observed (Fig. 3E). These aragonite structures have been described in the Altamira Cave, where they were associated with microbial communities in which *Streptomyces* was a dominant species[46]. Overall, these observations highlight the complexity of carbonate formation in subterranean environments, where microbial activity and physicochemical factors interact to produce diverse mineral structures.

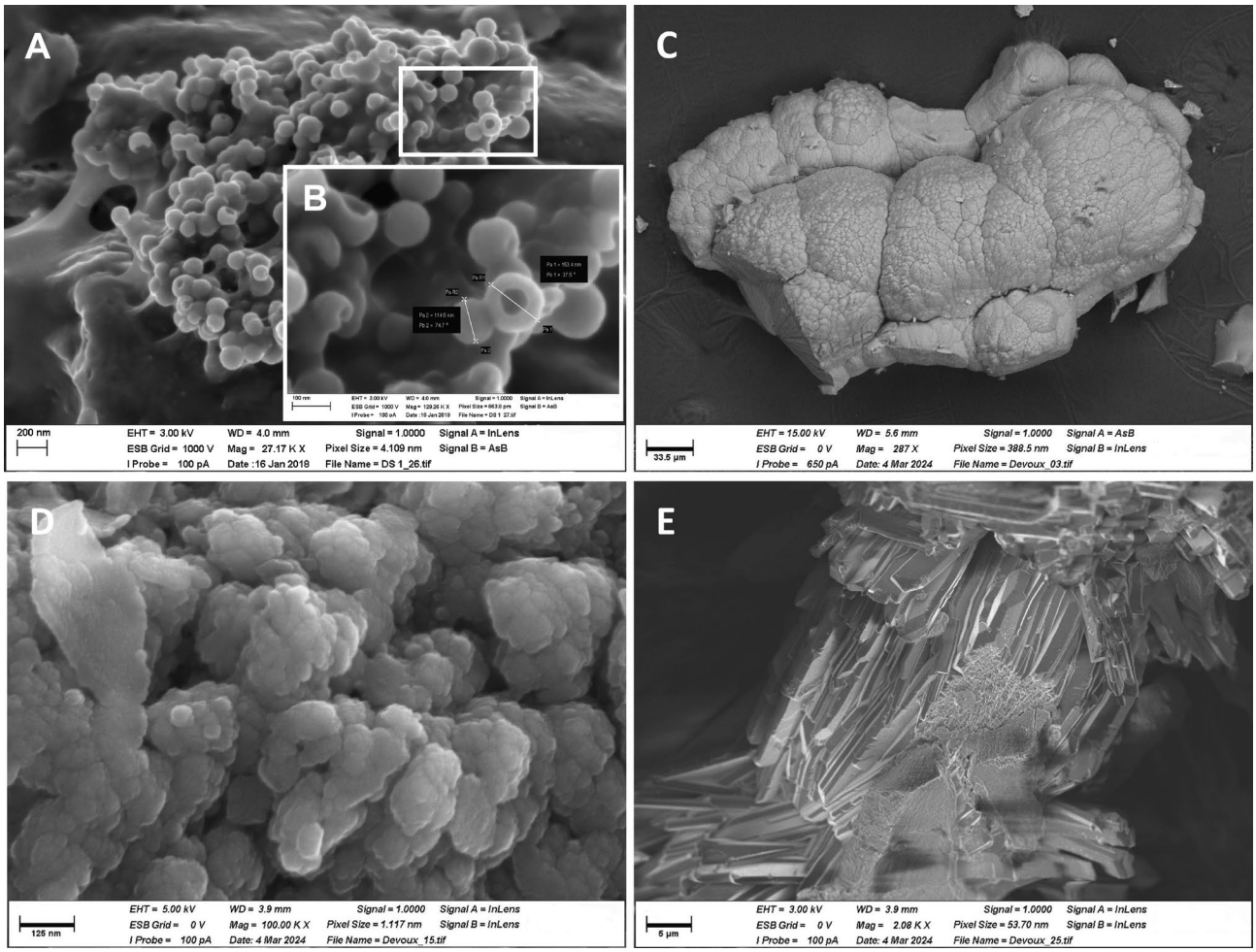

Fig. 3. FE-SEM micrographs for some crystal morphologies in Devaux cave**.** (**A**) Surface structure of a CCC from room G. (**B**) Magnification area and measurement of the structures shown in A. (**C**) Globular $CaCO_3$ of a CCC from room SPD (**D**) Magnification of surface of C. (**E**) $CaCO_3$ with prismatic habit of a CCC from room SPD.

Microbial diversity and community structure in Devaux cave

Metabarcoding analyses yielded a total of 9,343 ASVs across all samples (Tables S2 and S3), of which 8,696 were bacterial and 647 were microeukaryotic. All 16S rRNA gene amplicons were successfully assigned, whereas 340 eukaryotic ASVs (52.5%) remained unclassified, reflecting the limited reference databases for cave microeukaryotes. Rarefaction curves reached saturation for all samples (Fig. S3), confirming adequate sequencing depth. However, sample DEV-6 lacked 18S rRNA data due to insufficient DNA for both 16S and 18S amplification, a common limitation in low-biomass environments such as perennial ice deposits.

Bacterial community composition

Bacteria and archaea have been widely reported in icy cave ecosystems worldwide[47]. but the detection of microeukaryotes remains less frequent, despite their presence in other Pyrenean caves[15]. In Devaux Cave, Proteobacteria (40.8%), Actinobacteriota (22.9%), and Patescibacteria (15.7%) dominated the prokaryotic community structure (Fig. 4A), consistent with patterns observed in other cold, oligotrophic environments[47]. Firmicutes were abundant in DEV-4, suggesting localized niches that may favor spore-forming taxa under freeze–thaw dynamics.

At the genus level, marked differences emerged between sample types. *Lysobacter* dominated perennial ice samples (DEV-3 to DEV-6), whereas *Candidatus Nomurabacteria* prevailed in liquid water samples (DEV-1 and DEV-2) (Fig. 4B). This distribution likely reflects contrasting ecological strategies: *Lysobacter* species are known for their metabolic versatility and ability to degrade complex polymers, which may confer an advantage in nutrient-limited ice matrices[48]. Conversely, *Nomurabacteria* (*Patescibacteria*) are often associated with symbiotic or parasitic lifestyles, thriving in liquid microhabitats where host interactions are more feasible[49].

Cyanobacteria were scarce in perennial ice (DEV-4 and DEV-5) but abundant in liquid water and areas exposed to sunlight (DEV-1, DEV-2, and DEV-3), indicating a strong dependence on light availability and

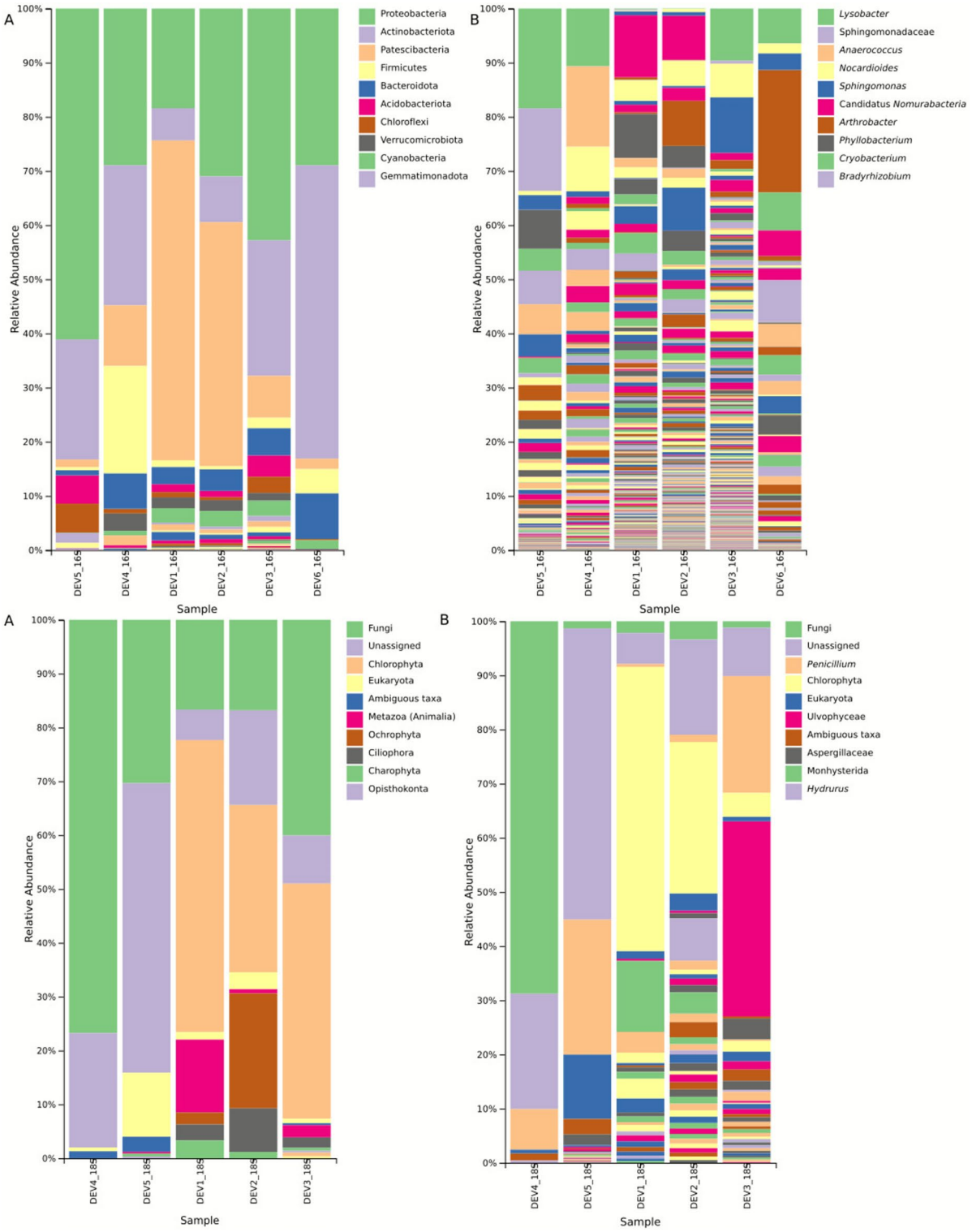

Fig. 4. Barplots representing the microbial community distribution in the Devaux cave samples at the phylum (**A**, **C**) and genus (**B**, **D**) levels. Relative abundances of major taxa of bacteria (**A**, **B**) and microeukaryotes (**C**, **D**) based on 16S rRNA and 18S rRNA gene sequencing data, respectively. The detailed taxonomy is summarized in Tables S2 and S3.

liquid-phase conditions for photosynthetic activity. This pattern mirrors observations in other karst systems, where phototrophic communities are restricted to entrance zones or drip waters[50].

Microeukaryotic diversity

Among eukaryotes, Opisthokonta (52.7%) and Archaeplastida (9%) were the most represented groups, although 30% of sequences remained unassigned (Fig. 4C), underscoring the presence of poorly characterized taxa in subterranean ecosystems. Fungal genera such as *Penicillium* and *Cladosporium* dominated (Fig. 4D), consistent with their role as decomposers in oligotrophic cave environments[51]. Notably, DEV-3, located near a partially sunny area, contained numerous sequences of green algae (Ulvophyceae), suggesting phototrophic colonization in transitional zones between aphotic and photic environments (Fig. S4).

Phylogenetic trees (Fig. 5) summarize the taxonomic placement of ASVs and their association with sample type. In addition to the phylogeny, this figure shows ASV taxonomic annotations at the genus and phylum levels, as well as the sample type in which each ASV was found. The bar size represents the confidence of the annotations. Several key differences were observed between the prokaryotic and eukaryotic phylogenies. While the vast majority of ASVs were annotated in the prokaryotic analysis, this was not the case in the eukaryotic analysis, where more than 50% of ASVs were annotated as "Unassigned," "D_0_Eukaryota," or "Ambiguous taxa." In the prokaryotic analysis, a large number of ASVs were found mainly in the liquid samples, especially those belonging to Patescibacteria, which represent the largest group. A higher proportion of eukaryotic ASVs were found in the perennial ice samples. Further analyses are needed to better understand the distribution of microbial communities, since these results do not take into account the relative abundance of the ASVs mentioned.

High fractions of unassigned eukaryotic metabarcodes have been reported elsewhere in cave and environmental datasets, largely reflecting incomplete eukaryotic reference databases and marker/primer biases (e.g., ITS/18S). Recent efforts to improve coverage, such as EUKARYOME and EukRibo, explicitly note that eukaryotic taxonomic assignment remains constrained by reference gaps, which can inflate "Unassigned" labels in complex environmental communities[52,53]. In fungal metabarcoding, pipeline and read-quality artifacts (particularly with ITS2) have also been shown to reduce assignment rates for specific taxa unless trimming/curation steps are optimized, offering a methodological explanation for elevated "Unassigned" calls. Comparable patterns have been documented in cave studies: for example, work in the Scărișoara Ice Cave demonstrates that eukaryotic communities in ice can be complex yet hard to resolve taxonomically, even when high-throughput sequencing is applied; metatranscriptomic profiling revealed diverse microeukaryotes but emphasized the analytical challenges of classification in frozen cave habitats[54]. In contrast, bacterial/archaeal assignments are often more complete due to mature rRNA repositories (e.g., SILVA), which helps explain the higher annotation success observed here for prokaryotes.

Metagenomic evidence and the "microbial dark matter"

Complementing metabarcoding, metagenomic sequencing of DEV-4 and DEV-5 yielded 33,835,762 reads, predominantly bacterial (8.9 million in DEV-4; 13.2 million in DEV-5). Taxonomic profiling revealed dominant phyla consistent with amplicon data, Proteobacteria, Actinobacteriota, and Patescibacteria, but also uncovered low-abundance lineages such as Chloroflexota, Acidobacteriota, and candidate phyla within the CPR (Candidate Phyla Radiation). These CPR taxa, often associated with reduced genomes and symbiotic lifestyles, exemplify the "microbial dark matter" in oligotrophic cave ice[16].

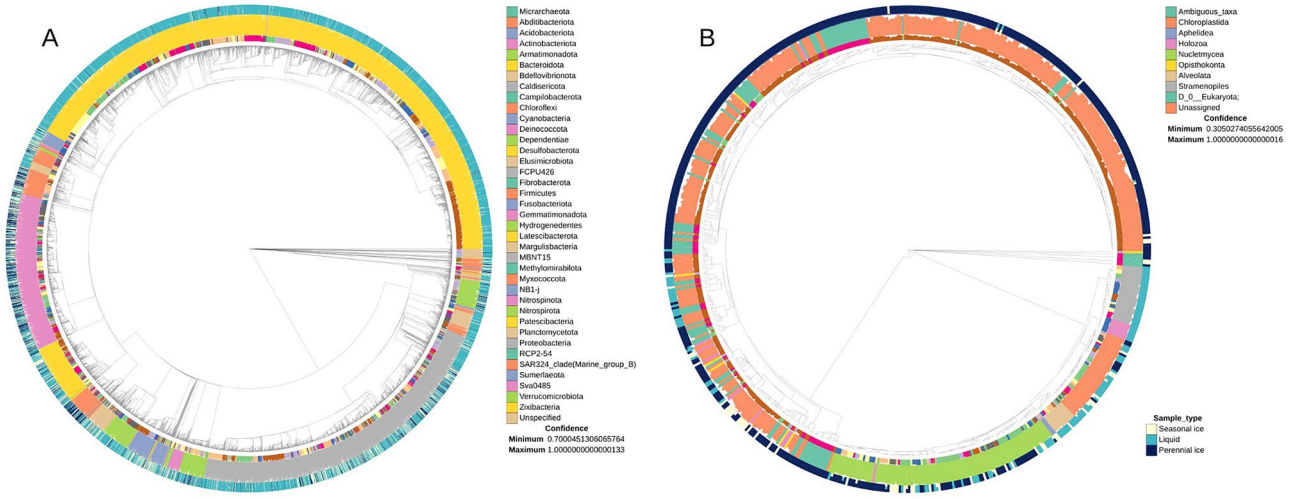

Fig. 5. Phylogenetic trees representing ASVs identified by 16S and 18S rRNA gene sequencing. The rings represent, from inside to outside: taxonomy at the genus level, taxonomy at the phylum level, sample type, sample name. (**A**) Bacteria. (**B**) Eukaryotes.

Functional annotation (via KEGG categories) indicated enrichment of genes linked to stress response, cold-adaptation (e.g., antifreeze proteins), and metabolic flexibility, including pathways for methane oxidation and sulfur cycling, suggesting ecological roles beyond those inferred from 16S profiles. Notably, DEV-5 harbored multiple contigs encoding glycosyl hydrolases and peptidases, consistent with polymer degradation strategies previously attributed to *Lysobacter* in ice samples (Bacterial Community Composition). Viral signatures (predominantly bacteriophages) and eukaryotic fragments were also detected, though at low coverage, reinforcing the complexity of these communities.

Despite these insights, a substantial fraction of reads remained unmapped (6.6 million and 3.8 million) or taxonomically unclassified (505,200 and 480,134), underscoring the limitations of current reference databases and the prevalence of novel lineages in cryospheric and subterranean ecosystems[55]. This observation aligns with global reports of metagenomes dominated by unknown taxa in extreme environments, where functional potential often exceeds taxonomic resolution. Together, these findings highlight that Devaux Cave harbors a reservoir of poorly characterized organisms whose metabolic capabilities remain largely speculative, emphasizing the need for integrative approaches combining metagenomics, single-cell genomics, and cultivation to illuminate this microbial dark matter.

Microbial diversity and community distribution

According to the gallery arrangement of the cave (Fig. 1C), sample DEV-5 was taken from the innermost ice body. In contrast, the other samples were more exposed to external variables such as ventilation and temperature oscillations (DEV-3, DEV-4, and DEV-6) or sunlight (DEV-3 and to a lesser extent DEV-6). In the bacterial analysis, this difference was revealed by the higher relative abundance of photosynthetic groups such as cyanobacteria in liquid samples (DEV-1 and DEV-2), and in seasonal ice samples (DEV-3 and DEV-6). In microeukaryotes, the same results were found (except DEV-6). Chlorophytes such as *Oogamochamys* and other photosynthesizing microorganisms such as the unicellular algal genus *Raphidonema* were identified[56].

Based on the cave's gallery configuration (Fig. 1C), sample DEV-5 was collected from the innermost ice body, whereas samples DEV-3, DEV-4, and DEV-6 were located closer to the entrance and thus more exposed to external factors such as ventilation and temperature fluctuations. Among these, DEV-3, and to a lesser extent DEV-6, also received seasonal sunlight. This gradient of exposure influenced microbial composition. Bacterial analysis revealed a higher relative abundance of photosynthetic taxa, particularly cyanobacteria, in liquid samples (DEV-1 and DEV-2) and in seasonal ice samples (DEV-3 and DEV-6), consistent with the role of light in promoting phototrophic communities in cave environments[57]. Similarly, microeukaryotic profiles showed comparable patterns, except for DEV-6, which exhibited lower phototroph representation. Chlorophytes such as *Oogamochamys* and unicellular green algae of the genus *Raphidonema*, both known for their photosynthetic capacity and adaptation to low-light or cryophilic habitats, were identified. These findings underscore the influence of light availability and microclimatic variability on microbial diversity within cave ice ecosystems[15,47].

Different geochemical features directly influence the existence of ecological niches in Devaux Cave, shaping microbial community structure across liquid water, seasonal ice, and perennial ice. These niches are determined by redox conditions, nutrient availability, and physical constraints such as mineral surfaces and ice matrices. Liquid water samples represent oxygenated, nutrient-enriched microhabitats where dissolved ions (Ca^{2+}, Mg^{2+}) and organic matter favor heterotrophic taxa, explaining the prevalence of Verrucomicrobiota and Bdellovibrionota, which are often associated with dynamic predator–prey interactions in oxic environments[58]. Seasonal ice creates transient niches with fluctuating redox gradients during freeze–thaw cycles, promoting taxa such as Actinobacteriota, Bacteroidota, and Firmicutes, which possess stress-response and spore-forming capabilities adapted to periodic oxygen limitation and osmotic stress[47]. In contrast, perennial ice represents an extreme oligotrophic niche characterized by low nutrient flux, stable low temperatures, and limited diffusion of gases. Here, Proteobacteria and Chloroflexi dominate, likely due to their metabolic versatility and ability to exploit trace organics or mineral-associated substrates[47]. Mineral surfaces embedded in ice may act as catalytic sites for chemolithotrophic processes, as observed in other cryospheric systems. Geochemical variables influencing these niches include ionic composition, which vary between liquid water and ice matrices. ANCOM-BC comparisons confirmed these ecological patterns (Fig. S5): Verrucomicrobiota and Bdellovibrionota were enriched in liquid samples, Actinobacteriota and Firmicutes in seasonal ice, and Proteobacteria and Chloroflexi in perennial ice. Cyanobacteria were more frequent in ice, where intermittent light exposure enables limited photosynthetic activity, as suggested by the green layers observed in sample DEV-3 (Fig. S4). These findings are consistent with previous studies in icy caves and permafrost environments, where geochemical gradients strongly correlate with microbial diversity and functional potential[59].

Among eukaryotes, photosynthetic Archaeplastida were almost equally present in liquid and seasonal ice samples, suggesting that light availability, even if limited, supports phototrophic taxa in both environments. This aligns with previous findings that green algae and related groups can persist under low-light or cryophilic conditions[57]. The slight overrepresentation of the heterogeneous SAR group in liquid samples may reflect their preference for more dynamic, nutrient-rich microhabitats, as many SAR members include heterotrophic or mixotrophic protists adapted to fluctuating conditions[47]. Opisthokonta, encompassing fungi, were more abundant in the ice sample DEV-3, which could indicate a role in organic matter decomposition or symbiotic interactions within biofilms, processes often enhanced in stable, low-light niches[15]. The higher proportion of ambiguous taxa in seasonal and especially perennial ice suggests the presence of poorly characterized or dormant forms, possibly linked to extreme oligotrophy and long-term isolation. Overall, these patterns point to light availability, nutrient flux, and microclimatic stability as key drivers shaping microeukaryotic communities in cave ice ecosystems. Seasonal ice, periodically exposed to sunlight and meltwater, favors phototrophs and mixotrophs, whereas perennial ice harbors more cryptic or stress-tolerant taxa, reflecting adaptation to persistent darkness and resource scarcity. Although statistical relevance is limited due to the small number

of samples, this method shows tendencies and suggests differences that can be confirmed by complementary analyses (e.g., barplots and ordination methods). The sampling inconveniences make it impossible to include a larger number of samples. Due to this limitation, statistical differences between groups were not computed. Positional clustering confirms the results suggested by direct representation of taxonomic annotations (e.g., barplots) and compositional analysis (e.g., ANCOM-BC).

After the evidence of differences between sample types, the dissimilarity in microbial diversity between samples was calculated using the Bray–Curtis dissimilarity metric. To investigate the phyla and genera driving these differences, a biplot was calculated and plotted (Fig. S6). Here, it was found that in both 16S and 18S rRNA analyses, liquid samples were quite similar to each other, whereas both perennial and seasonal ice samples were more different. This trend was less intense in bacterial communities, where ice samples were also close. In the level of phylum, the differences in the liquid samples were explained by the higher abundance of Patescibacteria and the absence of important groups such as Proteobacteria and Actinobacteriota. At the genus level, the high proportion of *Candidatus Nomurabacteria* drove the dissimilarities between sample types, which makes sense since this genus belongs to the phylum Patescibacteria. The seasonal ice samples differed from the other samples mainly by the high proportion of Actinobacteriota, but also by the low influence of Firmicutes and Bacteoidota. Notably, the perennial ice sample DEV-4 was more similar to these samples than to the other perennial ice sample. In this case, the absence of Actinobacteriota and the high proportion of Proteobacteria did differentiate DEV-5. These differences in samples were more noticeable when the computation included genera rather than phyla. The coordinate representing the genus *Arthrobacter*, representative of Actinobacteria provides similar information. This coordinate is key to differentiate seasonal ice samples DEV-3, and especially DEV-6 where this genus was very frequent. On the other hand, the coordinate driven by Proteobacteria is divided into its belonging groups: genus *Lysobacter*, frequent in both seasonal ice and perennial ice samples and unclassified ASVs of the family Sphingomonadaceae, almost specific to sample DEV-5. The last genus with special relevance was *Anaerococcus*, a gram-positive anaerobic bacterium belonging to Firmicutes that is almost specific to sample DEV-4 and drives the difference in this sample.

In the analysis of the microeukaryotes, the results were slightly different. The ordination patterns suggest that liquid samples, enriched in Stramenopiles and Chloroplastida, represent niches where motility and phototrophy confer adaptive advantages. Stramenopiles, many of which are flagellated heterotrophs or mixotrophs, likely benefit from the higher nutrient flux and dynamic conditions in liquid habitats[47]. Similarly, the presence of Chloroplastida in areas exposed to sunlight underscores the role of light as a selective force, consistent with phototrophic persistence in cryophilic environments. The perennial ice sample DEV-4, dominated by Nucletmycea (fungi), reflects a contrasting strategy: reliance on heterotrophy and organic matter recycling in stable, aphotic conditions. This divergence between Chloroplastida and Nucletmycea along the main ordination axes highlights niche partitioning driven by energy acquisition strategies and microclimatic stability. Unclassified ASVs, particularly in DEV-3 and DEV-5, introduce uncertainty but also point to unexplored diversity in extreme cave ice ecosystems. Rather than a mere limitation, this taxonomic ambiguity suggests the presence of novel or poorly characterized lineages adapted to oligotrophic, cryogenic conditions, an area warranting targeted phylogenetic and genomic studies. At the genus level, the influence of Ulvophyceae in seasonal ice and *Penicillium* in perennial ice further illustrates functional differentiation, with phototrophs exploiting transient light and fungi dominating in long-term dark habitats. These findings emphasize that microeukaryotic assemblages are structured by light availability, substrate stability, and resource gradients, reflecting both ecological filtering and potential evolutionary specialization in subterranean cryoenvironments.

To explore the relationship between microbial community composition and geochemical variables, two sets of CCA were performed. The first CCA included major anions quantified by ion chromatography (CO_3^{2-}, NO_3^-, SO_4^{2-}, PO_4^{3-}). This model explained 93.4% of the variance in prokaryotic community structure and 89.7% for eukaryotes, indicating a strong association between ionic gradients and microbial distribution (Fig. S6, S7; Table S4). The second CCA, based on ICP-MS elements (C, Ca, Cl, F, Fe, K, Mg, Na, P, S, Si, U), explained a lower proportion of variance, consistent with the weaker ecological signal of trace elements compared to major ions. This suggests that macro-ionic composition exerts a stronger control on microbial assemblages than trace metals, likely due to its role in osmotic balance and nutrient availability. These results support the interpretation that ion gradients act as key environmental filters, shaping both bacterial and microeukaryotic communities. Seasonal ice, enriched in SO_4^{2-} and NO_3^-, favored phototrophs and mixotrophs, whereas perennial ice, with lower ionic variability, harbored stress-tolerant heterotrophs and fungi.

Functional characteristics inferred from metataxonomy

Metataxonomic data were used to predict the relative abundance of functional characteristics (e.g., KEGG orthologs) within microbial communities, providing an approximation of their potential metabolic capabilities rather than direct functional evidence[60] (Tables S5 and S6). These predictions were generated using PICRUSt2, which infers functions based on similarity to reference genomes. It is important to note that this approach introduces uncertainty, particularly in poorly characterized or highly specialized communities, where reference coverage is limited. Therefore, the results should be interpreted as hypotheses about functional potential, not confirmed activities. To reduce noise and highlight dominant patterns, features with a relative abundance below 0.1% across all samples were excluded. While this filtering substantially reduced the number of predicted features, it allowed us to focus on those most likely to influence ecosystem-level processes.

Cluster analysis of the most abundant KOs revealed two main dendrogram structures: one grouping samples by similarity in KO frequencies (vertical) and another grouping features by their distribution across samples (horizontal) (Fig. S8A). Samples tended to cluster by type, suggesting that sample type may influence predicted metabolic potential. Seasonal ice and liquid samples were more similar to each other than to perennial ice samples. Horizontally, less abundant KOs were concentrated on the left side of the heatmap, where perennial ice

samples exhibited higher predicted frequencies compared to seasonal ice and liquid samples. More abundant features were located on the right, where differences among sample types were less pronounced.

Using KEGG pathway annotations[61], predicted KOs were categorized as follows: 39% metabolic pathways, 33% environmental information processing, 18% cellular processes, and 12% genetic information processing. The distribution was not uniform across clusters. For example, the right cluster was enriched in environmental information processing functions, particularly ABC transporters, including the most abundant predicted KO (K03088, RNA polymerase sigma-70 factor), which is associated with bacterial stress responses[62]. The left cluster contained most functions related to cellular processes and genetic information processing, suggesting variability in these categories among sample types. These patterns may indicate that membrane transport mechanisms are consistently important in extreme environments, although this inference remains speculative given the predictive nature of the analysis.

For microeukaryotic communities, clustering was less consistent with sample type (Fig. S8B). Seasonal ice and liquid samples showed similar patterns, but differentiation was limited, possibly due to low sequence coverage in sample DEV-6. Overall, perennial ice samples exhibited higher predicted KO frequencies than other sample types. Horizontal clustering revealed three zones: (i) a left cluster dominated by cellular process-related functions, (ii) a central cluster enriched in metabolic and genetic information processing functions, and (iii) a right cluster containing most environmental information processing features. These differences suggest potential functional specialization among sample types, but again, these are predictions based on taxonomic profiles, not direct measurements of gene expression or activity.

In summary, PICRUSt2-based predictions suggest that environmental information processing, particularly membrane transport, may represent a core functional trait in these communities, while other processes vary more across sample types. However, these findings should be interpreted cautiously, as they reflect inferred functional potential rather than experimentally validated functions, and biases are likely in underrepresented taxa.

Metabolic potential inferred from metagenomics

Functional prediction obtained from amplicon sequencing data can provide an overview of the metabolic potential of the microbial community and differences in metabolic potential as a function of metadata characteristics such as sample type. But if more reliable information on the functional structure of the community is required, shotgun metagenomics is a better approach, as functional profiles are not inferred from taxonomy, but from direct sequence alignment to a function database[63]. This means that it is possible to detect gene duplications, gene deletions or non-functional genes even if the same microbial taxa are identified by amplicon sequencing. Therefore, further analysis of the functional profiles of the bacterial, archaeal and eukaryotic communities was performed using shotgun metagenomics on perennial ice samples DEV-4 and DEV-5. These analyses provided insight into the metabolic potential of perennial ice samples, which are a type of ice that has been little studied. Samples DEV-4 and DEV-5 were selected for metagenomic analysis as they represent perennial ice, considered the most oligotrophic and stable niche within Devaux Cave. Both samples contained CCC, and the mechanisms underlying its formation remain poorly understood. Metagenomic sequencing was conducted to assess whether specific microbial taxa or metabolic pathways are associated with CCC formation, aiming to elucidate potential links between microbial activity and mineral precipitation processes in frozen cave environments. Furthermore, FE-SEM observations revealed the presence of precipitated minerals in these samples, suggesting a possible role of microorganisms in biomineralization processes (Fig. 3).

Carbon metabolism

The functional profiles were evaluated against the semi-closed, cryogenic pool environment of perennial ice, characterized by CO_2 degassing, solute enrichment, and limited organic inputs, under which stress-response and low-temperature metabolic pathways would be selectively maintained. Carbon metabolism comprises the most important pathways in cells and is involved in a long list of biological functions. In these analyses, several genes were found related to carbon pathways such as energy metabolism, carbon fixation, and methane metabolism.

Enzymes associated with acetogenesis and fermentation were detected. Although these processes are not represented as canonical pathways in KEGG, their underlying genetic circuits have been characterized in prior work on archaeal acetogenesis and methane-derived acetate production[64]. In the present analyses, reads mapped to K01905, which in KEGG corresponds to acdA, the α-subunit of acetate-CoA ligase, and reads also mapped to K22224, the β-subunit. Although the acd family was historically emphasized in archaea, archaeal-like ACDs have also been reported in bacteria, notably in *Chloroflexus aurantiacus*, where an ACD was identified[65]. Consequently, the assignment of acd-family reads to Bacteria, specifically Actinomycetota and Pseudomonadota, was unexpected but plausible, given the documented mosaic distribution of ACD across domains, likely shaped by horizontal gene transfer and subunit/domain rearrangements within the NDP-forming acyl-CoA synthetase superfamily[66]. In addition, multiple sequences for enzymes mediating the conversion of pyruvate to L-lactate and ethanol were identified, supporting fermentative capacity in the ice-cave microbial communities.

Sequences of three enzymes, 3-hydroxypropionyl-CoA synthetase, a 3-hydroxypropionyl-coenzyme A dehydratase, and a biotin carboxyl carrier protein (K18594, K15019, and K18605 respectively) were detected in the carbon fixation pathway and were taxonomically assigned to archaea (Fig. 6A). Two of these enzymes have no described bacterial equivalents, whereas K15019 shares similarity with K14469, a key enzyme in bacterial CO_2 fixation pathways[67]. Differences in metabolic potential between the two perennial ice samples were evident in the methane metabolism pathway (Fig. 6B). In DEV-4, several subunits of heterodisulfide reductase, an enzyme complex essential for methanogenesis, were present but underrepresented in DEV-5. Conversely, DEV-5 contained KO numbers linked to methanofuran biosynthesis and coenzyme M biosynthesis, which were absent or less abundant in DEV-4. These contrasts suggest that the two samples supported distinct strategies for

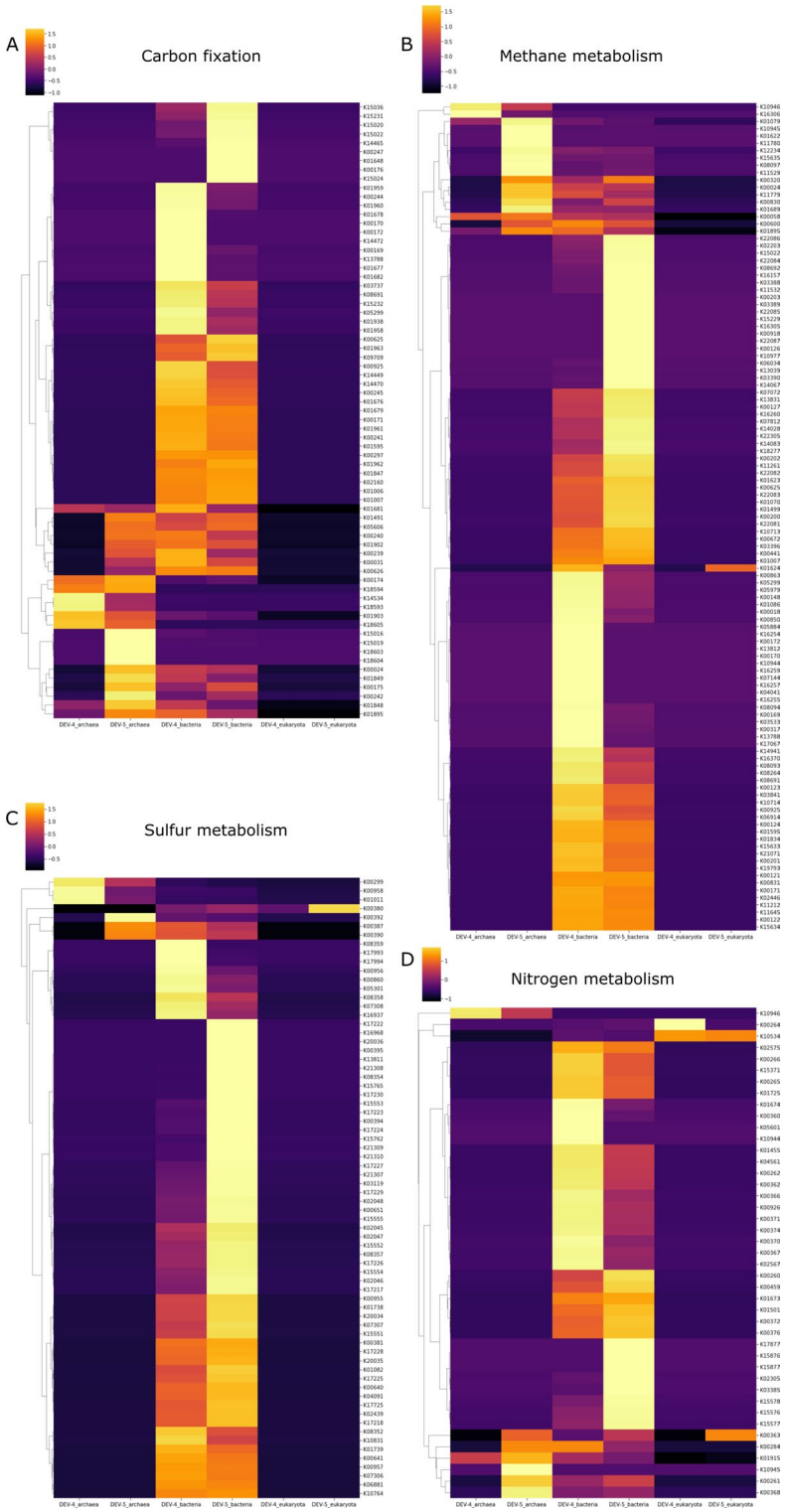

Fig. 6. Heatmap of relative abundance. Heat map showing the relative abundance of functions in microorganisms from perennial ice samples. Metabolic potentials were inferred from metagenomics. (**A**) Carbon fixation. (**B**) Methane metabolism. (**C**) Sulfur metabolism. (**D**) Nitrogen metabolism.

methane metabolism, reflecting microenvironmental variability within perennial ice. It has been documented that archaea and bacteria perform different reactions and influence microbial communities in distinct ways[68]. In this study, the observed divergence in methanogenesis-related genes between DEV-4 and DEV-5 demonstrated that metabolic strategies varied substantially within the same extreme permafrost environment, likely driven by local geochemical and physical heterogeneity.

Nitrogen metabolism

Nitrogen metabolism is central to cellular processes and ecologically relevant in ice-cave systems because it mediates nutrient cycling under oligotrophic conditions. Key pathways such as nitrate reduction, nitrification, denitrification, and nitrogen fixation have been documented in most ecosystems[69]. In this study, 43 KO identifiers associated with nitrogen metabolism were detected, covering major routes including assimilatory and dissimilatory nitrate reduction, denitrification, nitrogen fixation, and partial steps of nitrification and anammox (Fig. 6D). Differences in nitrogen metabolism were observed between taxonomic groups and sample types. In the eukaryotic subset, the presence of K10534 (NADPH-dependent nitrate reductase), which catalyzes nitrate reduction to ammonia in the assimilatory pathway, was notable (Fig. 6D). A similar trend was found for K10946, annotated as methane/ammonia monooxygenase, which was overrepresented in archaeal populations, particularly in DEV-4. This annotation was unexpected because previous reports describe this enzyme only in bacteria[70]. While horizontal gene transfer and gene conservation between bacteria and archaea have been documented[71], annotation bias or incomplete reference databases cannot be ruled out; further validation is required before confirming interdomain transfer.

At the bacterial level, clusters of functions with similar abundance (e.g., K02575, K00266, K15371, K00260) and clusters with contrasting abundance were identified. For example, K02305 (nitric oxide reductase subunit C), overrepresented in DEV-4, is a key component of the denitrification pathway. All denitrification functions were detected in both samples, but the higher abundance of specific KOs in DEV-4 suggests greater potential for this pathway in that sample. Genes encoding enzymes for assimilatory and dissimilatory nitrate reduction were also present, along with enzymes linking nitrogen metabolism to glutamate and arginine pathways.

Conversely, pathways such as anammox and nitrification were poorly reconstructed, indicating limited coverage and depth for these routes and suggesting low ammonia consumption in perennial ice. This interpretation is consistent with ion chromatography results, where ammonia concentrations were below detection limits (Table S1).

Sulfur metabolism

In Devaux Cave, sulfur cycling was investigated because sulfur occurs in waters, in cryogenic gypsum ($CaSO_4{\cdot}2H_2O$), and as sulfides (e.g., pyrite) in the bedrock[6]. *Achromatium*, a large sulfur-oxidizing gammaproteobacterium, has been reported to store elemental sulfur (S^0) granules that are subsequently oxidized to sulfate, and to accumulate intracellular $CaCO_3$ bodies that appear to buffer pH and link to sulfur oxidation dynamics at oxic-anoxic boundaries. Recent work indicates these carbonate inclusions are often amorphous calcium carbonate rather than crystalline calcite, and single-cell genomic studies have shown *Achromatium* encodes sulfur-oxidation and nitrogen/oxygen respiration functions consistent with a role in sediment sulfur cycling[58].

Sulfur participates in energy metabolism through three main routes: assimilatory sulfate reduction, which converts sulfate to sulfide for biosynthesis[72]; dissimilatory sulfate/sulfur reduction, where sulfate or sulfur act as terminal electron acceptors under anaerobic conditions[73]; and oxidation pathways, including the SOX system, which oxidizes thiosulfate to sulfate[74]. These processes were evaluated based on metagenomic evidence (Fig. 6C). Most sequences mapped to sulfur-related functions were assigned to Bacteria, but four KO identifiers, K00299 (FMN reductase), K00958 (sulfate adenylyltransferase), K01011 (thiosulfate sulfurtransferase), and K00392 (ferredoxin-dependent sulfite reductase), were detected in archaeal bins, despite being previously reported only in bacteria. This observation may reflect horizontal gene transfer, functional convergence, or annotation limitations due to incomplete archaeal representation in reference databases.

A marked difference in sulfur metabolism was observed between perennial ice samples. DEV-5 showed higher abundance of five enzymes involved in thiosulfate oxidation via the SOX complex, suggesting that this pathway was more prominent in this sample. In contrast, DEV-4 contained elevated levels of K17993 and K17994, encoding subunits of sulfhydrogenase, an enzyme originally characterized in the hyperthermophilic archaeon *Pyrococcus furiosus*, indicating potential for sulfur respiration[75]. Although *P. furiosus* was not detected taxonomically, similar findings have been reported in other cold environments, where thermophilic genes persist due to micro-scale thermal niches or dispersal rather than bulk temperature conditions[15,76].

Additional sequences related to assimilatory sulfate reduction and sulfate/thiosulfate transport systems were identified, along with ABC transporters for taurine and alkanesulfonates, linking substrate uptake to sulfur oxidation and assimilation. Among the three major routes, assimilatory sulfate reduction and the SOX system were the best reconstructed, particularly in DEV-5, whereas dissimilatory reduction was less complete except for the sulfhydrogenase signal in DEV-4.

Iron metabolism

Metallic ions are considered essential in global metabolism, functioning as enzyme cofactors, in cellular communication, and in energy processes[77]. Iron is regarded as one of the most significant elements due to its involvement in microbial redox reactions and its evolutionary relevance through Fe-S clusters, which are conserved catalytic motifs across taxa and thought to be among the earliest on Earth[78]. The role of iron depends on its oxidation state: Fe(III) is utilized as an electron donor under microanaerobic conditions, whereas Fe(II) serves as a terminal electron acceptor for iron-reducing bacteria and archaea[77,79]. However, iron can become harmful in frozen environments, where high concentrations occur in brines formed within ice veins. These niches may support microbial life but pose challenges for organisms lacking adaptive mechanisms such as specific transporters[80].

Among the functions identified in the dataset, several iron-related transporters were detected, including K02010, K02011, and K02012, which are components of the iron (III) transport system. In contrast, no annotated sequences associated with Fe-siderophore functions were observed. Siderophores are chelating

compounds employed by microorganisms to facilitate iron (III) uptake, as this oxidation state of the metal is poorly soluble at neutral pH[81]. The absence of siderophore-related functions may indicate a limited role for siderophore-mediated iron acquisition within these microbial populations; however, this interpretation should be approached with caution. This observation appears consistent with the low iron concentrations reported for these samples and for the Devaux ice cave as a whole (Table S1), which likely influences the diversity of iron transport mechanisms present. Nevertheless, several sequences encoding enzymes involved in iron (II) uptake were identified, including K04758 and K04759, which belong to the FeO transport system[82]. Additional enzymes classified as iron (II)/manganese transporters and zinc/manganese/iron (II) transporters were also detected. These non-specific transporters are responsible for the uptake of metals that may contribute to energy metabolism through redox processes.

Metagenome-assembled genomes (MAGs)

Based on metagenomic analyses, bacterial genomes were assembled, and a phylogenetic tree representing the 10 MAGs obtained is shown in Fig. S9. MAG recovery is influenced by multiple environmental and technical factors. In this study, the limited number of samples (n = 2) from an oligotrophic environment, combined with low biomass and DNA yield, made genome assembly particularly challenging.

Among the 10 MAGs recovered, only three could be classified at the genus level: *Cryobacterium*, *Pseudonocardia*, and *Phyllobacterium*, with estimated completeness values of 97.89%, 80.16%, and 65.93%, respectively. These genera are typically associated with cold-adapted environments and may contribute to carbon and nitrogen cycling through heterotrophic metabolism (*Cryobacterium*)[47], secondary metabolite production (*Pseudonocardia*)[17], and oligotrophic lifestyles (*Phyllobacterium*)[42]. The remaining MAGs were classified only at higher taxonomic ranks, reflecting the limited representation of these microorganisms in current reference databases. This lack of genomic characterization, combined with the metagenomic patterns observed, such as low diversity and incomplete metabolic repertoires, highlights the need for further exploration of perennial ice cores to improve understanding of microbial adaptation and ecosystem functioning in these extreme niches.

Bacteria-induced mineral precipitation (BIMP)

Microorganisms, particularly bacteria, are widely recognized as active agents in mineral precipitation through processes collectively known as BIMP. This phenomenon, well documented for carbonates, is influenced by factors such as cell density, ion concentration, diffusion, and pH, which together control ion supersaturation[73]. In cold, isolated environments like Devaux cave, limited cell mobility and nutrient diffusion may create microenvironments favorable for biomineralization[17].

Metagenomic analysis revealed metabolic pathways and enzymes potentially contributing to BIMP, supporting the hypothesis that microbial activity influences mineral formation within the cave (Fig. 7). Autotrophic pathways detected in DEV-4 and DEV-5, including phosphoenolpyruvate carboxylase and ribulose-1,5-bisphosphate carboxylase, can reduce CO_2 concentration and increase pH, conditions that favor carbonate precipitation under the alkaline cave environment (pH 7.2–9.1). Although these genes occur at low relative

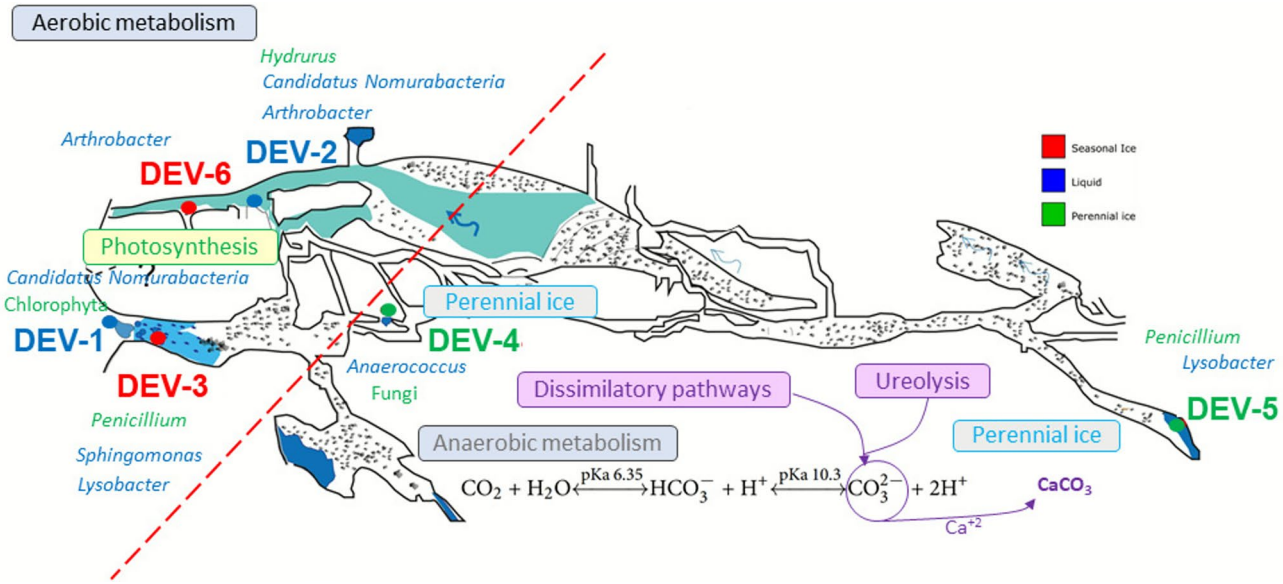

Fig. 7. The biogeochemical environment of Devaux cave. Graphical representation of the most representative genus in each sample (bacteria in blue, eukaryotes in green). The metabolic potential of microorganisms was strongly dependent on the nature of the sample (liquid water, seasonal ice, perennial ice). Autotrophic pathways cause a raise in pH and in carbonate concentration. This process combined with a high concentration of cations induce BIMP.

abundance, previous studies indicate that even modest autotrophic activity can affect carbonate equilibria in oligotrophic systems[29].

Additional evidence includes urease-related genes (K01428-K01430) and ammonia lyases (K01744-K01745), which locally increase pH and promote carbonate formation[83]. Ureolytic bacteria are recognized as key players in biomineralization; sequences were detected in genera such as *Bradyrhizobium* and *Phyllobacterium*, while *Halomonas*, previously linked to ureolytic activity, represented ~ 1.2% of sequences in DEV-4[84,85]. Morphological observations of globular forms in this sample resemble structures attributed to *Halomonas*[86], although this association remains hypothetical.

Carbonic anhydrase (K01672), an enzyme directly catalyzing carbonate formation from CO_2 and water, was also identified. Pathways related to nitrogen and sulfur cycles were partially reconstructed, including dissimilatory nitrate reduction, which can generate ammonia, and assimilatory sulfate reduction (Fig. 8). These processes may indirectly influence carbonate and sulfate mineral precipitation, consistent with the detection of calcite, aragonite, vaterite, and nesquehonite, minerals previously associated with microbial mediation in similar environments[17,27,87].

Although cyanobacteria, often implicated in gypsum biomineralization[87], were rare (0.015%), the presence of diverse taxa and functional genes suggests that multiple microbial strategies may contribute to mineral formation over long timescales. In summary, while gene abundances are low and direct functional validation is lacking, combined metagenomic and mineralogical evidence supports the occurrence of BIMP in Devaux cave. These processes are likely slow and spatially heterogeneous, but the presence of key metabolic pathways and associated minerals indicates that microorganisms may play a significant role in shaping mineral landscape of the cave.

Finally, viral reads were detected in perennial ice samples, but their role in biomineralization remains speculative. Previous studies suggest that viruses can act as nucleation sites for mineral precipitation, initially through permineralization by amorphous magnesium silicates and later transforming into magnesium carbonate nanospheres during diagenesis[88]. In Devaux cave, dissolved Mg^{2+} and Ca^{2+} from surrounding rocks could support such processes; however, no direct evidence is currently available, and this possibility should be considered a perspective for future research.

Conclusions

This study provides an integrated genomic overview of microbial communities in the Devaux ice cave, indicating that extreme cryogenic conditions and microclimatic gradients shape diversity and potential functionality. Comparisons among liquid water, seasonal ice, and perennial ice suggest that each habitat represents a distinct ecological niche structured by light, ionic composition, and substrate stability.

Key contributions include: (i) Adaptation in cryoenvironments: Assemblages exhibit traits consistent with survival under oligotrophic, low-temperature, and low-light conditions; (ii) Unexplored diversity: A high proportion of unclassified ASVs highlights the need for improved taxonomic frameworks and genomic resources; (iii) Tentative biogeochemical roles: Metagenomic inference points to pathways linked to carbon and nitrogen cycling and possible biomineralization, though these remain speculative and require experimental validation.

Future research should address methodological limitations through higher sequencing depth, increased sample number, and targeted functional assays, to bridge the gap between genomic potential and ecological function.

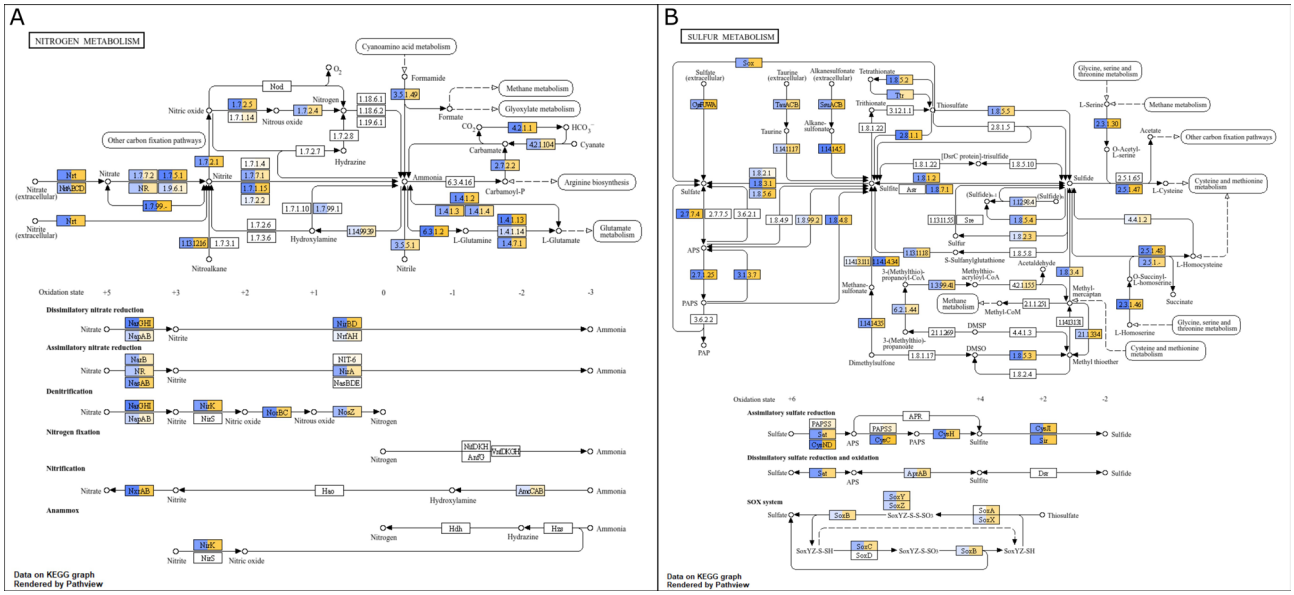

Fig. 8. Reconstruction of metabolic pathways from the metagenome. (**A**) Nitrogen metabolism (**B**) Sulfur metabolism. The colored boxes correspond to the enzymes identified in this study. The intensity of the color represents the relative abundance of that function. Blue: sample DEV-4. Yellow: sample DEV-5.

Sample	Type of sample	Location	Description	Metataxonomy*	Metagenomics
DEV-1	Liquid	Porche entrance	Water from a drip located immediately at cave entrance	+	-
DEV-2	Liquid	Gallery between room F and Brulle Spring	Water from the river inside the cave	+	-
DEV-3	Seasonal ice	Porche entrance	Ice core from the firn at cave entrance ("Porche" entrance). Sunny area affected by important thermal oscillations. Ice results from a mix of snow, congelation of drip water, thaw-freezing cycles and sublimation. The ice shows greenish areas	+	-
DEV-4	Perennial ice	Room SPD	Ice core taken from the ice body located ~ 80 m from cave entrance. Massive ice with radial bubbles and CCC (Bartolomé et al., 2023)	+	+
DEV-5	Perennial ice	Room K	Ice core from the ice body located ~ 280 m from cave entrance. Massive and pristine ice with CCC	+	+
DEV-6	Seasonal ice	Brulle Spring	Important thermal oscillations. Seasonal ice formed by the freezing of the river when the cave outlet is dammed in during winter-spring	+	-

Table 1. Name, type of sample, location, description and genomic analysis of the samples. * (+, test performed -, test not performed).

Beyond its local context, this work contributes to understanding microbial resilience in extreme environments, offering analogs for icy ecosystems on Earth and potentially extraterrestrial settings. Future research should prioritize higher sequencing depth, increased sample number, and targeted experiments (e.g., functional assays and cultivation) to bridge the gap between genomic potential and ecological function.

Materials and methods

Study area and Devaux cave

Devaux Cave (~ 2836 m a.s.l.) is located on the eastern cliff of the Gavarnie Cirque (France) within the Monte Perdido Massif, which includes Monte Perdido Peak (3355 m a.s.l.), the highest calcareous (non-metamorphic) mountain in Europe (Fig. 1A). The region lies in a transitional zone between Atlantic and Mediterranean climatic influences. The zero-degree isotherm, assuming a lapse rate of 0.55–0.65 °C per 100 m, is near 2950 m a. s. l[89]., close to the cave's altitude (Fig. 1B). Maximum snow accumulation occurs in April, exceeding 3 m near the Monte Perdido Glacier, ~ 3 km east of the cave[90]. Discontinuous permafrost predominates between 2750 and 2900 m a.s.l., with probable permafrost above 2900 m on north-facing slopes[91,92]. The subnival zone (2800–3355 m a.s.l.) supports sparse vegetation dominated by pioneer species such as *Androsace ciliata*, *Saxifraga pubescens*, *Cerastium alpinum*, and *Linaria alpina*[93].

Cave deposits include clastic, chemical (CCC, cryogenic cave gypsum, and speleothems), and ice deposits[6], with most cryogenic minerals still embedded in ice. Monitoring (2011–2021) revealed two thermal regimes: (i) large seasonal fluctuations and air temperatures above 0 °C near the entrance and main gallery, influenced by advective airflow and heat from the cave river; and (ii) stable temperatures below 0 °C in the interior, controlled by heat conduction through bedrock (Fig. 1C). Permafrost above the cave is estimated at ~ 200 m thick and extends ~ 350 m toward the southern face of the massif. It likely reflects a combination of present rock undercooling by cave ventilation and remnants from colder periods[6]. During late winter and early spring, frozen outlets dam water, forming a temporary lake in room F (Fig. 1C). Perennial ice bodies may have originated during past episodes of prolonged sealing and freezing, indicating colder or longer damming events than those observed today[6].

Ice drilling and sampling

A summary of the overall experimental strategy is represented in Fig. S10. Ice and water samples were collected from the cave environment. Ice samples were thawed and subsequently filtered to isolate microbial cells. The filtrate was used for chemical analyses, whereas the retained microorganisms were processed for microscopic examination and subjected to DNA extraction for downstream genomic analyses.

Six samples were analyzed (Table 1): two liquid water samples (DEV-1 from a dripping point at the Porche entrance and DEV-2 from the cave river) and four ice cores. Liquid samples were collected in sterile 2L bottles, kept cold, and stored at − 20 °C until processing. Ice cores (DEV-3 to DEV-6) were obtained using a 30 cm stainless-steel auger coupled to a battery drill, wrapped in sterile plastic, and transported frozen. DEV-3 (firn) was collected near the Porche entrance, an area subject to annual snow accumulation, melt-refreeze cycles, and occasional algal blooms (Fig. S4). DEV-6 represented seasonal layered ice formed during late winter/early spring 2022 due to Brulle Spring blockage. These were classified as seasonal ice. DEV-4 and DEV-5, sampled from pristine perennial ice in rooms SPD and K, were taken from marginal zones to minimize impact and classified as perennial ice. This classification into firn, seasonal ice, and perennial ice provides a framework to address the main research questions on how contrasting cryogenic habitats influence microbial diversity, functional potential, and biogeochemical roles within the cave ecosystem.

All samples were transported at −20 °C from the field to the laboratory at the Centro de Astrobiología (Madrid, Spain). Then, ice samples were decontaminated following previously described procedures[59]. Each section of the ice core was removed from −20 °C and washed with 0.22 µm-filtered MilliQ water. The ice samples were allowed to thaw and the meltwater was filtered separately through filters with pores of 0.22 µm attached to a vacuum pump in a flow hood, previously disinfected with ethanol. Both filters and meltwater were used for DNA

extraction and chemical analysis respectively (Fig. S1). To control laboratory contamination, sterile MilliQ water was subjected to the same analytical processes. All laboratory steps were performed under aseptic conditions, using a UV-irradiated laminar flow hood, ethanol-cleaned tools, and sterilized gloves.

Chemical analysis of samples

Water samples for chemical analysis were acidified with ultrapure nitric acid to achieve a final concentration of approximately 2% (v/v), ensuring stabilization of dissolved metals and preventing their precipitation.

Assays for anions (fluoride, lactate, acetate, formate, chloride, nitrate, phosphate, sulfate, and carbonate) and cations (sodium, ammonium, potassium, magnesium, calcium, and strontium) from each filtered meltwater sample were performed by ion chromatographic method using suppressed conductivity detection in an 861 Advance Compact IC system (Metrohm AG, Herisau, Switzerland) using previously established procedures[94].

Chromatograms were recorded using the Metrohm IC Net 2.3 SR4 software. The system was run in the isocratic mode with the columns Metrosep A Supp 7 250/4,0 and Metrosep C3 250/4,0 at 45 °C. Ions were identified and quantified with internal and external standards prepared from Certified Standard Solutions (TraceCERT®) (Merck). Three sampling replicates were analyzed at each sample point.

Carbonate determination was carried out using the carbonate hardness test with the RQFlex® 10 Reflectometer from MERCK.

Concentrations of trace elements in liquid and ice samples (Al, B, Ba, Br, C, Ca, Cl, Cu, Fe, I, K, LI, Mg, Mn, Mo, Na, P, S, Se, Si, Sr, U, and Zn) were analyzed by inductively coupled plasma-mass spectrometry (ICP-MS) on a Perkin Elmer ELAN9000 ICP-MS quadrupole spectrometer[59]. Quantitative ICP-MS analysis was carried out using an external standard calibration approach. The analytical sequence included a blank (1% HNO_3, Suprapur®, Merck), a series of external standards at different concentrations, the samples, and a quality control standard at the end to monitor instrumental drift and potential memory effects. Rhodium (Rh) was added as an internal standard to blanks, standards, and samples. External calibration and quality control standards were prepared from two multi-element stock solutions (1000 mg L^{-1}): Multi-element Calibration Standard 2 (Perkin-Elmer) and ICP Multi-element Standard Solution VI Certipur® (Merck), both containing all analyzed elements. Three sampling replicates were analyzed at each sample point.

Statistical analyses

Statistical differences in the ion concentrations among samples were tested under ANOVA, preceded by a normality check and followed by Bartlett's test for equal variances using GraphPad Prism version 7.0 (GraphPad Software, La Jolla California USA, www.graphpad.com). All data were expressed as mean ± SD of three sampling replicates.

The effects of the chemical composition of samples on the microbial community composition were investigated by Canonical Correspondence Analyses (CCA) developed with CANOCO 5 software (Microcomputer Power, Ithaca)[95–97]. Monte Carlo tests with 500 permutations were run.

X-ray Diffraction

X-ray Diffraction (XRD) analyses were conducted on CCC from the ice surface and over a block from room SPD and room C-SPD (Fig. 3C) following established procedures[6]. These analyses were developed at the Geosciences Institute in Barcelona (GEO3-BCN-CSIC) using a Bruker-AXS D5005 powder diffractometer, using Cu K_α radiation, on randomly oriented powders. The XRD scans were recorded between 4° and 60° in 2θ with a 0.035° step size and equivalent acquisition times of 384 s. Identification was carried out using the JCPDS Powder Diffraction File as a Data Reference. Semi-quantitative phase analyses were performed using the reference intensity ratio (RIR) method. For this purpose, RIR values available in the PDF-2 database were employed. These analyses aimed to identify carbonate polymorphs and other cryogenic minerals, providing mineralogical context for interpreting microbial roles in biomineralization within the cave.

Field Emission Scanning Electron Microscopy (FE-SEM)

FE-SEM analyses were conducted at the Servicios de Apoyo a la Investigación (SAI), University of Zaragoza (Spain), using a Carl Zeiss MERLIN microscope. Samples of CCC from rooms D, G, and SPD were prepared by coating with platinum for morphological observations or with carbon when energy-dispersive X-ray spectrometry (EDS) was also required. The operational parameters (magnification, voltage, detector) are indicated in the images. Magnification range was 200× −130,000×. FE-SEM was used to identify putative microbial structures, while EDS analyses determined the elemental composition of selected features; carbon coating, instead of platinum, was used in this case to avoid interferences from the coating metal.

Extraction, quantification and sequencing of DNA

The DNA from each 0.22 µm pore filter was extracted and purified with a DNeasy PowerWater Kit (Qiagen, Germany). DNA concentration was determined using a Qubit fluorometer (Thermo Fisher Scientific, USA), using the High Sensitivity kit. The amplification and sequencing of the V3-V4 regions of the 16S rRNA gene (forward sequence CCTACGGGNGGCWGCAG; reverse sequence GACTACHVGGGTATCTAATC) were performed to identify bacteria[98]. Microeukaryotes were identified by amplification and sequencing of the V4-V5 regions of the 18S rRNA gene (forward sequence GCCAGCAVCYGCGGTAAY; reverse sequence CCGTCAATTHCTTYAART)[94]. The sequencing procedure was performed on Illumina MiSeq 2 × 250–2 × 300, to obtain approximately 100,000 reads per sample. Paired-end reads were obtained.

Further, metagenomic analyses were performed on the perennial ice samples (DEV-4 and DEV-5) to determine the genome structure of the entire population in these samples. Shotgun libraries were prepared by the TruSeq system and also sequenced on Illumina MiSeq (2.4 Gb). Paired-end reads were obtained.

Metataxonomy data analysis and prediction of metabolic pathways from taxonomy

Data analysis of both 16S rRNA and 18S rRNA amplicon sequencing was performed in parallel using Qiime2 (v2023.2)[99] to process the reads obtained from the sequencing and acquire taxonomic, phylogenetic and diversity results.

Preprocessing and quality control

The primers from 16S rRNA amplicons were removed with the CUTADAPT tool (via q2-cutadapt)[100]. Then, reads were processed with DADA2 (via q2-dada2)[101] to obtain the representative sequences and the amplicon sequence variants (ASV) table using the following parameters: –p-trunc-len-f 245 –p-trunc-len-r 196 for 16S rRNA amplicons. These sets of parameters permitted the retention of high-quality reads from the forward sequences and the elimination of low-quality sequences, especially from the reverse reads. For 18S rRNA amplicons: –p-trunc-len-f 0 –p-trunc-len-r 0. In this case, primers were not removed beforehand in order to maintain the minimum overlapping region.

Taxonomic annotation

Taxonomic annotations were performed using the classify-sklearn method from the feature-classifier Qiime2 plugin. Naïve-Bayes trained classifiers were used in this step. SILVA reference database was used to train the classifiers (release 138–99-nr for 16S rRNA amplicons and 132–99-nr for 18S rRNA amplicons)[102,103]. For phylogenic analysis, the align-to-tree-mafft-iqtree method was used[104]. It generates a MAAFT alignment and then infers a phylogenic tree with IQ-tree starting from the masked alignment. Visualization of these results was generated with the EMPress plugin[105].

Diversity and functional inference

Bray–Curtis distance matrices and Principal Coordinate Analysis (PCoA) were calculated using the core-metrics-phylogenetic method. Rarefaction was applied with sampling depths of 146,076 for 16S rRNA and 5,633 for 18S rRNA to avoid sample loss. Differences in taxonomic composition among sample types (liquid, ice, or permafrost) were assessed using ANCOM-BC tests[106], considering genera and phyla with a minimum frequency of 1% in at least one sample. The significance threshold was set at $p < 0.01$. PCoA biplots were generated from Bray–Curtis matrices and feature tables collapsed by taxonomy to identify taxa contributing to dissimilarity.

Functional inference from metataxonomy was performed using PICRUSt2[60] within Qiime2. This tool predicts metabolic pathways and functional features (e.g., K numbers) from ASVs by assigning reference genomes, providing an overview of potential biochemical processes in each environment. It is important to note that these predictions are not direct measurements of metabolic activity and do not replace shotgun metagenomics. To retain the most relevant features, abundance and prevalence thresholds were applied: for 16S rRNA, K numbers with ≥ 0.1% relative abundance in all samples; for 18S rRNA, ≥ 0.01% in at least four of five samples. Only these features were used for subsequent analyses and visualizations.

Functional inference

The prediction of functional features from metataxonomy was conducted using the Qiime2 adapted version of Phylogenetic Investigation of Communities by Reconstruction of Unobserved States (PICRUSt2)[60]. This program allows the inference of functional features (i. e. K numbers) from ASVs by the assignment of a reference genome. In studies where DNA quantity is scarce, this tool can give an overall picture of the metabolic potential of microbial communities but it is important to highlight that these functional annotations are not direct observations of metabolic potential and do not replace shotgun metagenomics. In order to select the most relevant K numbers, both the abundance and prevalence thresholds were employed. In the 16S rRNA analysis only those K numbers with a minimum relative abundance of 0.1% in all samples were retained. In the 18S rRNA analysis, the threshold chosen was a minimum abundance of 0.01% in four out of the five samples. Only these retained features were considered for further analyses and visualizations.

Metagenomics data analysis and prediction of metabolic pathways from metagenomics

The metagenomics data were analyzed with SqueezeMeta v1.6.2[107]. Assembly was done using Megahit[108]. Short contigs (< 200 bps) were removed and contig statistics were done with Prinseq[109]. RNAs were predicted using Barrnap[110]. The 16S and 18S rRNA sequences were taxonomically classified using the RDP classifier[111]. ORFs were predicted using Prodigal[112]. The alignment of sequencing reads against the protein reference databases GenBank[113], eggNOG[114], and KEGG[115] was done in March 2023 using the algorithm Diamond[63]. Similarity searches for HMM homology searches were done by HMMER3[116] for the Pfam database[117]. Read mapping against contigs was performed using Bowtie2[118]. Bin statistics were computed using CheckM[119].

The prediction of pathways from metagenomics was conducted using MinPath[120]. KEGG[115] and MetaCyc[121] pathway databases included in MinPath were updated as of May 10, 2021. These results were analyzed using custom Python and Rscripts which include the SQMtools package[122]. The reconstruction of metabolic pathways from the metagenome were represented using the open source R package Pathview included in the SqueezeMeta pipeline[123]. Medium quality bins (contamination below 10% and completeness above 50%) were considered MAGs[124].

Metagenomic analysis of perennial ice samples is constrained by several factors, including limited sample availability and low DNA concentration in the ice cores. Consequently, sequencing replicates could not be included in this study. Given that only two samples were sequenced, some aspects of downstream analyses, such as co-assembly and bin reconstruction, are inherently limited in resolution and should be interpreted accordingly.

Nucleotide sequence accession numbers

Sequences obtained by 16S rRNA and 18S rRNA sequencing and by shotgun metagenomics have been deposited in the NCBI Short Read Archive (SRA), BioProject PRJNA1099162.

Data availability

Sequences obtained by 16S rRNA and 18S rRNA sequencing and by shotgun metagenomics have been deposited in the NCBI Short Read Archive (SRA), BioProject PRJNA1099162.

Received: 30 July 2025; Accepted: 21 January 2026
Published online: 26 January 2026

References

1. Vidaller, I. et al. Toward an Ice-Free Mountain Range: Demise of Pyrenean Glaciers During 2011–2020. *Geophysical Research Letters* **48**, e2021GL094339 (2021).
2. Biskaborn, B. K. et al. Permafrost is warming at a global scale. *Nat Commun* **10**, 264 (2019).
3. Perşoiu, A. & Lauritzen, S. E. *Ice Caves*. https://doi.org/10.1016/c2016-0-01961-7. (Elsevier) 2018
4. Perşoiu, A. et al. Holocene winter climate variability in Central and Eastern Europe. *Sci Rep* **7**, 1–8 (2017).
5. Sancho, C. et al. Middle-to-late Holocene palaeoenvironmental reconstruction from the A294 ice-cave record (Central Pyrenees, northern Spain). *Earth Planet. Sci. Lett.* **484**, 135–144 (2018).
6. Bartolomé, M. et al. Mountain permafrost in the Central Pyrenees: insights from the Devaux ice cave. *Cryosphere* **17**, 477–497 (2023).
7. Luetscher, M., Jeannin, P.-Y. & Haeberli, W. Ice caves as an indicator of winter climate evolution: a case study from the Jura Mountains. *The Holocene* **15**, 982–993 (2005).
8. Racine, T. M. F., Reimer, P. J. & Spötl, C. Multi-centennial mass balance of perennial ice deposits in Alpine caves mirrors the evolution of glaciers during the Late Holocene. *Sci Rep* **12**, 11374 (2022).
9. Racine, T. M. F., Spötl, C., Reimer, P. J. & Čarga, J. Radiocarbon constraints on periods of positive cave ice mass balance during the last millennium, Julian Alps (NW Slovenia). *Radiocarbon* **64**, 333–356 (2022).
10. Spötl, C., Koltai, G. & Dublyansky, Y. Mode of formation of cryogenic cave carbonates: Experimental evidence from an Alpine ice cave. *Chem. Geol.* **638**, 121712 (2023).
11. Stoffel, M., Luetscher, M., Bollschweiler, M. & Schlatter, F. *Switzerland. Quat. res.* **72**, 16–26 (2009).
12. Žák, K. et al. Coarsely crystalline cryogenic cave carbonate – a new archive to estimate the Last Glacial minimum permafrost depth in Central Europe. *Clim. Past* **8**, 1821–1837 (2012).
13. Feurdean, A., Perşoiu, A., Pazdur, A. & Onac, B. P. Evaluating the palaeoecological potential of pollen recovered from ice in caves: A case study from Scărişoara Ice Cave. *Romania. Review of Palaeobotany and Palynology* **165**, 1–10 (2011).
14. Leunda, M. et al. Ice cave reveals environmental forcing of long-term Pyrenean tree line dynamics. *J. Ecol.* **107**, 814–828 (2019).
15. Ruiz-Blas, F. et al. The hidden microbial ecosystem in the perennial ice from a Pyrenean ice cave. *Front. Microbiol.* **14**, 1110091 (2023).
16. Jiao, J.-Y. et al. Microbial dark matter coming to light: challenges and opportunities. *National Science Review* **8**, nwaa280 (2021).
17. Lange-Enyedi, N. T., Németh, P., Borsodi, A. K., Spötl, C. & Makk, J. Calcium carbonate precipitating extremophilic bacteria in an Alpine ice cave. *Sci Rep* **14**, 2710 (2024).
18. Wind, M., Obleitner, F., Racine, T. & Spötl, C. Multi-annual temperature evolution and implications for cave ice development in a sag-type ice cave in the Austrian Alps. *Cryosphere* **16**, 3163–3179 (2022).
19. Spötl, C., Fohlmeister, J., Reimer, P. & Zhang, H. First insights into the age of the giant ice deposits in the Eisriesenwelt cave (Austria). *Sci Rep* **14**, 11001 (2024).
20. Wang, Y. et al. Synthesis, characterization and mechanism of porous spherical nesquehonite by CO2 biomimetic mineralization. *Adv. Powder Technol.* **33**, 103856 (2022).
21. Pacelli, C., Cassaro, A. & Zinzi, A. Unlocking the Potential of Caves in the Solar System: Targets for Life Detection, Deep-Space Exploration, and Human Outpost. *Space Sci Rev* **221**, 87 (2025).
22. Tebo, B. M. et al. Microbial communities in dark oligotrophic volcanic ice cave ecosystems of Mt Erebus. *Antarctica. Front. Microbiol.* **6**, 179 (2015).
23. Žák, K. *et al.* Cryogenic Mineral Formation in Caves. in *Ice Caves* 123–162 https://doi.org/10.1016/b978-0-12-811739-2.00035-8 (Elsevier, 2018).
24. Seixas, M. H., Munroe, J. S. & Eggleston, E. M. Bacterial diversity and geomicrobiology of Winter Wonderland ice cave, Utah, USA. *MicrobiologyOpen* **13**, e1426 (2024).
25. Jones, B. Microbes in caves: agents of calcite corrosion and precipitation. *Geological Society, London, Special Publications* **336**, 7–30 (2010).
26. Cacchio, P. et al. Involvement of Bacteria in the Origin of a Newly Described Speleothem in the Gypsum Cave of Grave Grubbo (Crotone, Italy). *JCKS* **74**, 7–18 (2012).
27. Meier, A. et al. Calcium carbonates: induced biomineralization with controlled macromorphology. *Biogeosciences* **14**, 4867–4878 (2017).
28. Enyedi, N. T. et al. Cave bacteria-induced amorphous calcium carbonate formation. *Sci Rep* **10**, 8696 (2020).
29. Zhu, T. & Dittrich, M. Carbonate Precipitation through Microbial Activities in Natural Environment, and Their Potential in Biotechnology: A Review. *Front. Bioeng. Biotechnol.* **4**, 4 (2016).
30. Ojha, A., Bandyopadhyay, T. K., Das, D. & Dey, P. Microbial Carbonate Mineralization: A Comprehensive Review of Mechanisms, Applications, and Recent Advancements. *Mol Biotechnol* https://doi.org/10.1007/s12033-025-01433-5 (2025).
31. Bartolomé, M. et al. Characteristics of cryogenic carbonates in a Pyrenean ice cave (northern Spain). *Geogaceta* **58**, 107–110 (2015).
32. Koltai, G., Spötl, C., Jarosch, A. H. & Cheng, H. Cryogenic cave carbonates in the Dolomites (northern Italy): insights into Younger Dryas cooling and seasonal precipitation. *Clim. Past* **17**, 775–789 (2021).
33. Luetscher, M., Borreguero, M., Moseley, G. E., Spötl, C. & Edwards, R. L. Alpine permafrost thawing during the Medieval Warm Period identified from cryogenic cave carbonates. *Cryosphere* **7**, 1073–1081 (2013).
34. Spötl, C., Koltai, G., Jarosch, A. H. & Cheng, H. Increased autumn and winter precipitation during the Last Glacial Maximum in the European Alps. *Nat Commun* **12**, 1839 (2021).
35. Žák, K., Onac, B. P. & Perşoiu, A. Cryogenic carbonates in cave environments: A review. *Quatern. Int.* **187**, 84–96 (2008).
36. Munroe, J. et al. Cryogenic cave carbonate and implications for thawing permafrost at Winter Wonderland Cave, Utah, USA. *Sci Rep* **11**, 6430 (2021).
37. Perşoiu, A., Onac, B. P., Wynn, J. G., Bojar, A.-V. & Holmgren, K. Stable isotope behavior during cave ice formation by water freezing in Scărişoara Ice Cave. *Romania. J. Geophys. Res.* **116**, D02111 (2011).
38. Spötl, C. & Koltai, G. Cryogenic cave carbonates: New insights from alpine ice caves. *Chem. Geol.* **685**, 122808 (2025).

39. Spötl, C. & Cheng, H. Holocene climate change, permafrost and cryogenic carbonate formation: insights from a recently deglaciated, high-elevation cave in the Austrian Alps. *Clim. Past* **10**, 1349–1362 (2014).
40. Teehera, K. B. et al. Cryogenic Minerals in Hawaiian Lava Tubes: A Geochemical and Microbiological Exploration. *Geomicrobiol J.* **35**, 227–241 (2018).
41. Ulloa-Cedamanos, F. et al. A Forty-Year Karstic Critical Zone Survey (Baget Catchment, Pyrenees-France): Lithologic and Hydroclimatic Controls on Seasonal and Inter-Annual Variations of Stream Water Chemical Composition, pCO2, and Carbonate Equilibrium. *Water* **12**, 1227 (2020).
42. Lange-Enyedi, N. T. et al. Calcium Carbonate Precipitating Cultivable Bacteria from Different Speleothems of Karst Caves. *Geomicrobiol J.* **39**, 107–122 (2022).
43. Joshi, S. & Banerjee, S. Ultrastructural analysis of calcite crystal patterns formed bybiofilm bacteria associated with cave speleothems. *J Microsc Ultrastruct* **2**, 217 (2014).
44. Cacchio, P. et al. Involvement of Microorganisms in the Formation of Carbonate Speleothems in the Cervo Cave (L'Aquila-Italy). *Geomicrobiol J.* **21**, 497–509 (2004).
45. Wang, H. et al. Calcium carbonate precipitation induced by a bacterium strain isolated from an oligotrophic cave in Central China. *Front. Earth Sci. China* **4**, 148–151 (2010).
46. Canaveras, J. C. et al. Microbial Communities Associated With Hydromagnesite and Needle-Fiber Aragonite Deposits in a Karstic Cave (Altamira, Northern Spain). *Geomicrobiol J.* **16**, 9–25 (1999).
47. Itcus, C. et al. Bacterial and archaeal community structures in perennial cave ice. *Sci Rep* **8**, 15671 (2018).
48. De Bruijn, I. et al. Comparative genomics and metabolic profiling of the genus Lysobacter. *BMC Genomics* **16**, 991 (2015).
49. Lemos, L. N. et al. Genomic signatures and co-occurrence patterns of the ultra-small Saccharimonadia (phylum CPR/Patescibacteria) suggest a symbiotic lifestyle. *Mol. Ecol.* **28**, 4259–4271 (2019).
50. Joanna, C.-M. & Andrzej, M. Diversity of Cyanobacteria on Limestone Caves. in *Cyanobacteria* (ed. Tiwari, A.) https://doi.org/10.5772/intechopen.79750 (InTech, 2018).
51. Cunha, A. O. B. et al. Living in the dark: Bat caves as hotspots of fungal diversity. *PLoS ONE* **15**, e0243494 (2020).
52. Tedersoo, L. et al. EUKARYOME: the rRNA gene reference database for identification of all eukaryotes. *Database* **2024**, baae043 (2024).
53. Kyle, K. E. & Klassen, J. L. Untrimmed ITS2 metabarcode sequences cause artificially reduced abundances of specific fungal taxa. *Appl Environ Microbiol* **91**, e01537-e1624 (2025).
54. Mondini, A. et al. High-throughput sequencing of fungal communities across the perennial ice block of Scărișoara Ice Cave. *Ann. Glaciol.* **59**, 134–146 (2018).
55. Rinke, C. et al. Insights into the phylogeny and coding potential of microbial dark matter. *Nature* **499**, 431–437 (2013).
56. Segawa, T. et al. Evolution of snow algae, from cosmopolitans to endemics, revealed by DNA analysis of ancient ice. *ISME J.* **17**, 491–501 (2023).
57. Joanna, C.-M. & Andrzej, M. 2018. Diversity of Cyanobacteria on Limestone Caves. in *Cyanobacteria* (ed. Tiwari, A.) https://doi.org/10.5772/intechopen.79750 (InTech, 2018).
58. Madigan, M. T., Martinko, J. M., Bender, K. S., Buckley, D. H. & Stahl, D. A. *Brock. Biología de Los Microorganismos*. (J. M. Nakagawa, Ed. Pearson Education) (2015).
59. Martinez-Alonso, E. et al. Taxonomic and functional characterization of a microbial community from a volcanic englacial ecosystem in Deception Island. *Antarctica. Sci Rep* **9**, 12158 (2019).
60. Douglas, G. M. et al. PICRUSt2 for prediction of metagenome functions. *Nat Biotechnol* **38**, 685–688 (2020).
61. Kanehisa, M., Furumichi, M., Sato, Y., Kawashima, M. & Ishiguro-Watanabe, M. KEGG for taxonomy-based analysis of pathways and genomes. *Nucleic Acids Res.* **51**, D587–D592 (2023).
62. Rhodius, V. A., Suh, W. C., Nonaka, G., West, J. & Gross, C. A. Conserved and Variable Functions of the σE Stress Response in Related Genomes. *PLoS Biol* **4**, e2 (2005).
63. Buchfink, B., Xie, C. & Huson, D. H. Fast and sensitive protein alignment using DIAMOND. *Nat Methods* **12**, 59–60 (2015).
64. Yang, S. et al. Genomic and enzymatic evidence of acetogenesis by anaerobic methanotrophic archaea. *Nat Commun* **11**, 3941 (2020).
65. Schmidt, M. & Schönheit, P. Acetate formation in the photoheterotrophic bacterium *Chloroflexus aurantiacus* involves an archaeal type ADP-forming acetyl-CoA synthetase isoenzyme I. *FEMS Microbiol Lett* **349**, 171–179 (2013).
66. Weiße, R.H.-J., Faust, A., Schmidt, M., Schönheit, P. & Scheidig, A. J. Structure of NDP-forming Acetyl-CoA synthetase ACD1 reveals a large rearrangement for phosphoryl transfer. *Proc. Natl. Acad. Sci. U.S.A.* **113**, e519-28 (2016).
67. Zarzycki, J., Brecht, V., Müller, M. & Fuchs, G. Identifying the missing steps of the autotrophic 3-hydroxypropionate CO2 fixation cycle in *Chloroflexus aurantiacus*. *Proc. Natl. Acad. Sci. U.S.A.* **106**, 21317–21322 (2009).
68. Bräsen, C., Esser, D., Rauch, B. & Siebers, B. Carbohydrate Metabolism in Archaea: Current Insights into Unusual Enzymes and Pathways and Their Regulation. *Microbiol Mol Biol Rev* **78**, 89–175 (2014).
69. Martínez-Espinosa, R. M., Cole, J. A., Richardson, D. J. & Watmough, N. J. Enzymology and ecology of the nitrogen cycle. *Biochem. Soc. Trans.* **39**, 175–178 (2011).
70. Norton, J. M., Alzerreca, J. J., Suwa, Y. & Klotz, M. G. Diversity of ammonia monooxygenase operon in autotrophic ammonia-oxidizing bacteria. *Arch Microbiol* **177**, 139–149 (2002).
71. Koonin, E. V. & Wolf, Y. I. Genomics of bacteria and archaea: the emerging dynamic view of the prokaryotic world. *Nucleic Acids Res.* **36**, 6688–6719 (2008).
72. Jespersen, M. & Wagner, T. Assimilatory sulfate reduction in the marine methanogen Methanothermococcus thermolithotrophicus. *Nat Microbiol* **8**, 1227–1239 (2023).
73. Hoffmann, T. D., Reeksting, B. J. & Gebhard, S. Bacteria-induced mineral precipitation: a mechanistic review. *Microbiology* **167**, 001049 (2021).
74. Rother, D., Henrich, H.-J., Quentmeier, A., Bardischewsky, F. & Friedrich, C. G. Novel Genes of the sox Gene Cluster, Mutagenesis of the Flavoprotein SoxF, and Evidence for a General Sulfur-Oxidizing System in Paracoccus pantotrophus GB17. *J Bacteriol* **183**, 4499–4508 (2001).
75. Ma, K., Weiss, R. & Adams, M. W. W. Characterization of Hydrogenase II from the Hyperthermophilic Archaeon Pyrococcus furiosus and Assessment of Its Role in Sulfur Reduction. *J Bacteriol* **182**, 1864–1871 (2000).
76. Milojevic, T., Cramm, M. A., Hubert, C. R. J. & Westall, F. "Freezing" Thermophiles: From One Temperature Extreme to Another. *Microorganisms* **10**, 2417 (2022).
77. McAllister, S. M., Vandzura, R., Keffer, J. L., Polson, S. W. & Chan, C. S. Aerobic and anaerobic iron oxidizers together drive denitrification and carbon cycling at marine iron-rich hydrothermal vents. *ISME J.* **15**, 1271–1286 (2021).
78. Braymer, J. J., Freibert, S. A., Rakwalska-Bange, M. & Lill, R. Mechanistic concepts of iron-sulfur protein biogenesis in Biology. *Biochimica et Biophysica Acta (BBA): Molecular Cell Research* **1868**, 118863 (2021).
79. Frey, P. A. & Reed, G. H. The Ubiquity of Iron. *ACS Chem. Biol.* **7**, 1477–1481 (2012).
80. Price, P. B. A habitat for psychrophiles in deep Antarctic ice. *Proc. Natl. Acad. Sci. U.S.A.* **97**, 1247–1251 (2000).
81. Katoh, H., Hagino, N., Grossman, A. R. & Ogawa, T. Genes Essential to Iron Transport in the Cyanobacterium Synechocystis sp. Strain PCC 6803. *J Bacteriol* **183**, 2779–2784 (2001).
82. Wyckoff, E. E., Mey, A. R., Leimbach, A., Fisher, C. F. & Payne, S. M. Characterization of Ferric and Ferrous Iron Transport Systems in Vibrio cholerae. *J Bacteriol* **188**, 6515–6523 (2006).

83. Reeksting, B., Paine, K. & Gebhard, S. In-depth profiling of calcite precipitation by environmental bacteria reveals fundamental mechanistic differences with relevance to application. Access Microbiology **1**, (2019).
84. Achal, V., Pan, X. & Zhang, D. Bioremediation of strontium (Sr) contaminated aquifer quartz sand based on carbonate precipitation induced by Sr resistant Halomonas sp. *Chemosphere* **89**, 764–768 (2012).
85. Martin, D., Dodds, K., Butler, I. B. & Ngwenya, B. T. Carbonate Precipitation under Pressure for Bioengineering in the Anaerobic Subsurface via Denitrification. *Environ. Sci. Technol.* **47**, 8692 (2013).
86. Rivadeneyra, M. A., Delgado, G., Ramos-Cormenzana, A. & Delgado, R. Biomineralization of carbonates by Halomonas eurihalina in solid and liquid media with different salinities: crystal formation sequence. *Res. Microbiol.* **149**, 277–287 (1998).
87. Thompson, J. B. & Ferris, F. G. Cyanobacterial precipitation of gypsum, calcite, and magnesite from natural alkaline lake water. *Geol* **18**, 995 (1990).
88. Pacton, M. et al. Viruses as new agents of organomineralization in the geological record. *Nat Commun.* **5**, 4298 (2014).
89. López-Moreno, J. I. et al. Thinning of the Monte Perdido Glacier in the Spanish Pyrenees since 1981. *Cryosphere* **10**, 681–694 (2016).
90. López-Moreno, J. I. et al. Ground-based remote-sensing techniques for diagnosis of the current state and recent evolution of the Monte Perdido Glacier. *Spanish Pyrenees. J. Glaciol.* **65**, 85–100 (2019).
91. Serrano, E. et al. Periglacial environments and frozen ground in the central Pyrenean high mountain area: Ground thermal regime and distribution of landforms and processes. *Permafrost & Periglacial* **30**, 292–309 (2019).
92. Serrano, E. et al. Frozen ground and periglacial processes relationship in temperate high mountains: a case study at Monte Perdido-Tucarroya area (The Pyrenees, Spain). *J. Mt. Sci.* **17**, 1013–1031 (2020).
93. Väre, H., Lampinen, R., Humphries, C. & Williams, P. Taxonomic Diversity of Vascular Plants in the European Alpine Areas. in Alpine Biodiversity in Europe (eds Nagy, L., Grabherr, G., Körner, C. & Thompson, D. B. A.) **167** 133–148 (Springer, 2003).
94. Garcia-Lopez, E. et al. Microbial Communities in Volcanic Glacier Ecosystems. *Front. Microbiol.* **13**, 825632 (2022).
95. Gloor, G. B., Macklaim, J. M., Pawlowsky-Glahn, V. & Egozcue, J. J. Microbiome Datasets Are Compositional: And This Is Not Optional. *Front. Microbiol.* **8**, 2224 (2017).
96. Leps, J. & Smilauer, P. *Multivariate Analysis of Ecological Data Using CANOCO* (Cambridge University Press, 2003).
97. Ter Braak, C. J. F. & Šmilauer, P. CANOCO. Software for Canonical Community Ordination. (Microcomputer Power, 2002).
98. Herlemann, D. P. R. et al. Transitions in bacterial communities along the 2000 km salinity gradient of the Baltic Sea. *ISME J.* **5**, 1571–1579 (2011).
99. Bolyen, E. et al. Reproducible, interactive, scalable and extensible microbiome data science using QIIME 2. *Nat Biotechnol* **37**, 852–857 (2019).
100. Martin, M. Cutadapt removes adapter sequences from high-throughput sequencing reads. *EMBnet j.* **17**, 10 (2011).
101. Callahan, B. J. et al. DADA2: High-resolution sample inference from Illumina amplicon data. *Nat Methods* **13**, 581–583 (2016).
102. Quast, C. et al. The SILVA ribosomal RNA gene database project: improved data processing and web-based tools. *Nucleic Acids Res.* **41**, D590–D596 (2012).
103. Yilmaz, P. et al. The SILVA and "All-species Living Tree Project (LTP)" taxonomic frameworks. *Nucl. Acids Res.* **42**, D643–D648 (2014).
104. Minh, B. Q. et al. IQ-TREE 2: New Models and Efficient Methods for Phylogenetic Inference in the Genomic Era. *Mol. Biol. Evol.* **37**, 1530–1534 (2020).
105. Cantrell, K. et al. EMPress Enables Tree-Guided, Interactive, and Exploratory Analyses of Multi-omic Data Sets. *MSystems.* **6**, 10–128 (2021).
106. Mandal, S. et al. Analysis of composition of microbiomes: a novel method for studying microbial composition. *Microbial Ecology in Health & Disease* **26**, 27663 (2015).
107. Tamames, J. & Puente-Sánchez, F. SqueezeMeta. A Highly Portable, Fully Automatic Metagenomic Analysis Pipeline. *Front. Microbiol.* **9**, 3349 (2019).
108. Li, D., Liu, C.-M., Luo, R., Sadakane, K. & Lam, T.-W. MEGAHIT: an ultra-fast single-node solution for large and complex metagenomics assembly via succinct *de Bruijn* graph. *Bioinformatics* **31**, 1674–1676 (2015).
109. Schmieder, R. & Edwards, R. Quality control and preprocessing of metagenomic datasets. *Bioinformatics* **27**, 863–864 (2011).
110. Seemann, T. Prokka: rapid prokaryotic genome annotation. *Bioinformatics* **30**, 2068–2069 (2014).
111. Wang, Q., Garrity, G. M., Tiedje, J. M. & Cole, J. R. Naïve Bayesian Classifier for Rapid Assignment of rRNA Sequences into the New Bacterial Taxonomy. *Appl Environ Microbiol* **73**, 5261–5267 (2007).
112. Hyatt, D. et al. Prodigal: prokaryotic gene recognition and translation initiation site identification. *BMC Bioinformatics* **11**, 119 (2010).
113. Clark, K., Karsch-Mizrachi, I., Lipman, D. J., Ostell, J. & Sayers, E. W. GenBank. *Nucleic Acids Res* **44**, D67–D72 (2016).
114. Huerta-Cepas, J. et al. eggNOG 4.5: a hierarchical orthology framework with improved functional annotations for eukaryotic, prokaryotic and viral sequences. *Nucleic Acids Res.* **44**, D286–D293 (2016).
115. Kanehisa, M. KEGG: Kyoto Encyclopedia of Genes and Genomes. *Nucleic Acids Res.* **28**, 27–30 (2000).
116. Eddy, S. R. A new generation of homology search tools based on probabilistic inference. in Genome Informatics. https://doi.org/10.1142/9781848165632_0019 (Published by imperial college press and distributed by world scientific publishing co., 2009).
117. Finn, R. D., Clements, J. & Eddy, S. R. HMMER web server: interactive sequence similarity searching. *Nucleic Acids Res.* **39**, W29–W37 (2011).
118. Langmead, B. & Salzberg, S. L. Fast gapped-read alignment with Bowtie 2. *Nat Methods* **9**, 357–359 (2012).
119. Parks, D. H., Imelfort, M., Skennerton, C. T., Hugenholtz, P. & Tyson, G. W. CheckM: assessing the quality of microbial genomes recovered from isolates, single cells, and metagenomes. *Genome Res.* **25**, 1043–1055 (2015).
120. Ye, Y. & Doak, T. G. A Parsimony Approach to Biological Pathway Reconstruction/Inference for Genomes and Metagenomes. *PLoS Comput Biol* **5**, e1000465 (2009).
121. Caspi, R. et al. The MetaCyc database of metabolic pathways and enzymes. *Nucleic Acids Res.* **46**, D633–D639 (2018).
122. Puente-Sánchez, F., García-García, N. & Tamames, J. SQMtools: automated processing and visual analysis of 'omics data with R and anvi'o. *BMC Bioinformatics* **21**, 358 (2020).
123. Luo, W. & Brouwer, C. Pathview: an R/Bioconductor package for pathway-based data integration and visualization. *Bioinformatics* **29**, 1830–1831 (2013).
124. The Genome Standards Consortium et al. Minimum information about a single amplified genome (MISAG) and a metagenome-assembled genome (MIMAG) of bacteria and archaea. *Nat Biotechnol.* **35**:725–731. 2017

Acknowledgements

We thank the directorates of the Parc National des Pyrénées (France) and the Parque Nacional de Ordesa y Monte Perdido (Spain) for their permission to investigate Devaux cave. We are indebted to Maria Paz Martin Redondo and to Miguel Ángel Lominchar from the Centro de Astrobiología for the ICP-MS analysis and for the ion chromatography analysis respectively. The analysis of the next-generation sequencing (NGS) was performed by the Parque Científico de Madrid. Our acknowledge to the Servicio General de Apoyo a la Investigación, SAI, Universidad de Zaragoza, Spain. We thank Paula Alcazar for reading this manuscript and for her helpful

revisions. We thank Ayuntamiento de Fanlo (https://www.fanlo.es/) for facilitate the access by the Las Cutas track (Nerín), Góriz hut staff (http://www.goriz.es), and the Palazio family (http://www.hotelpalazio.com) for their help during the fieldwork and sample transportation. We thank to Eduardo Bartolomé and Jose Esteban Lozano (https://mantenimientosmoncayo.com/) for auger design and construction. This study contributes to the work carried out by the DGA research groups Procesos Geoambientales y Cambio Global (ref. E02-20R) and GeoTransfer (E32_23), and the MERS research group 2017 SGR 1588. This research is part of POLARCSIC activities.

Author contributions

CC and MB designed the study and wrote the manuscript. AM led the scientific project (grant 2552/2020, ORCHESTRA). VMH, EGL, and CC generated the data and conducted the analysis. MB, RG, and GC participated in the sampling strategy and fieldwork. MCO arranged the samples for FE-SEM analysis. All authors participated in the interpretation of the results. All authors reviewed, commented and edited the manuscript.

Funding

This research was funded by grants PID2023-146641NB-C21 and MDM-2017–0737 Unidad de Excelencia "Maria de Maeztu"- Centro de Astrobiología (INTA-CSIC) by the Spanish Ministry of Science and Innovation/State Agency of Research MCIN/AEI/https://doi.org/10.13039/501100011033; and grant OCHESTRA ref. 2552/2020 by the National Parks Autonomous Agency (OAPN). Miguel Bartolomé is supported by a HORIZON-MSCA-2022-PF-01 (01107943). Eva Garcia-Lopez is recipient of a Fellowship (PTA2022-021737-I).

Declaration

Competing interests

The authors declare no competing interests.

Additional information

Supplementary Information The online version contains supplementary material available at https://doi.org/10.1038/s41598-026-37305-4.

Correspondence and requests for materials should be addressed to C.C.